Implementation of Geometry Dependent Charge Flux into Polarizable AMOEBA+ Potential

Chengwen Liu, † Jean-Philip Piquemal, †,‡,§ and Pengyu Ren †,*

[†] Department of Biomedical Engineering, The University of Texas at Austin, Austin, TX 78712, USA [‡] Laboratoire de Chimie Théorique, Sorbonne Université, UMR7616 CNRS, Paris, France [§] Institut Universitaire de France, 75005, Paris, France **ABSTRACT**

Molecular dynamics (MD) simulations employing classical force fields (FFs) have been widely

used to model molecular systems. The important ingredient of the current FFs, atomic charge,

remains fixed during MD simulations despite the atomic environment or local geometry changes.

This approximation hinders the transferability of the potential being used in multiple phases. Here

we implement a geometry dependent charge flux (GDCF) model into the multipole-based

AMOEBA+ polarizable potential. The CF in the current work explicitly depends on the local ge-

ometry (bond and angle) of the molecule. To our knowledge, this is the first study that derives

energy and force expressions due to GDCF in a multipole-based polarizable FF framework. Due

to the inclusion of GDCF, the AMOEBA+ water model is noticeably improved in terms of de-

scribing the monomer properties, cluster binding/interaction energy and a variety of liquid prop-

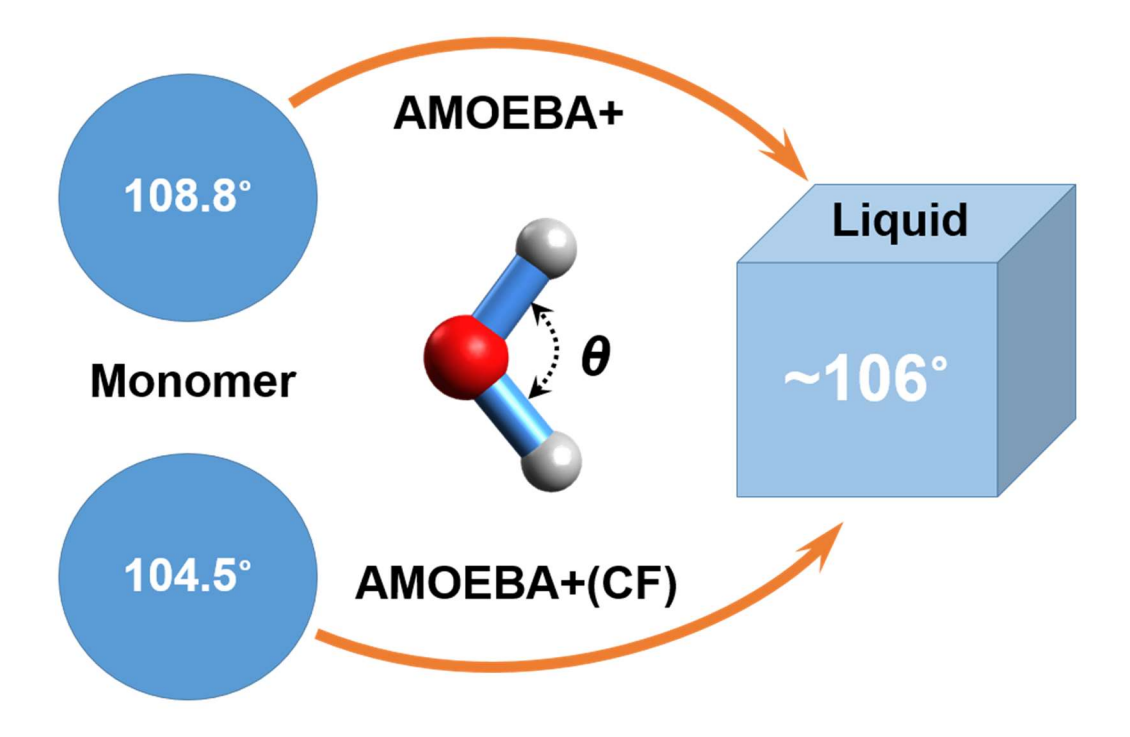
erties, including the infrared spectra that previous flexible water models were not able to capture.

KEYWORDS: Geometry dependent charges, AMOEBA+ potential, Polarizable water model, In-

frared spectra

TOC GRAPHICS

Geometry Dependent Charge Flux



Classical force fields (FFs) are commonly used to describe inter- and intramolecular interactions in molecular dynamics (MD) simulations. In popular fixed charge FFs, the atomic charges remain fixed during simulations. It is well understood however charges distributions are affected by both chemical environments through polarization effect and local geometry changes. The former is explicitly treated in "polarizable" FFs such as Drude oscillator, 2 atomic induced dipole, 3 and fluctuating charge models, where the charges can be calculated from the energy equilibration, 4-6 or bond capacity model.⁷ The latter is ignored by almost all classical FFs even though it is well known it causes issues. For example, the HOH angle of water in gas (104.5),8 liquid (~106)9 and ice (~109.5°)¹⁰ cannot be described consistently by common flexible model models. 11-12 This is due to incorrect dipole derivative of these flexible water models, without accounting for intramolecular charge transfer or charge flux (CF) when water geometry changes. The spectroscopically determined force field (SDFF) electrostatics by Krimm and co-workers was one of the few FFs that adopt a CF contribution. 13-15 Their study showed that CF is not only the key to the water angle opening from an isolated water molecule to its liquid phase but also helps in describing the conformational potential energy surface of the peptide. 13 TTM-family models by Xantheas and coworkers are other examples that incorporate CF effect. 16-17 Both the SDFF and TTM models show the necessity of incorporating CF for successfully describing vibrational spectroscopy which requires an accurate description of the molecular dipole surface. 11, 13-17 Dinur pointed out that CF is a first-order contribution to the electrostatic force in general and should not be neglected in MD simulations for flexible molecules. 12 Dinur and Hagler proposed a geometry dependent charge flux (GDCF) model, where atomic charges are explicitly dependent on the local geometry (bond, angle and torsion), for a series of small organic molecules. Based on the molecular dipole moments of organic molecules and amino acids calculated with density functional theory and point-charge FFs,

Jensen and coworkers concluded that the majority (~85 %) of the conformational dependence of molecular dipole moments can be attributed to the pure geometry effect and the remainder should be explicitly modeled by GDCF model. ¹⁸⁻¹⁹ Thus they suggested an inclusion of CF contribution from bond, angle and dihedral for developing more transferable FFs. By contrast, Dinur and Hagler demonstrated that CF due to bonds and angles is much more significant than that from dihedral. ²⁰

AMOEBA (Atomic Multipole Optimized Energetics for Biomolecular Applications) FF uses multipoles up to quadrupole to describe electrostatics and induced dipole to capture the non-additive many-body effect.^{3, 21-24} AMOEBA+ potential was developed very recently, where the "shortrange" physics including charge penetration ²⁵ and intermolecular charge transfer²⁶ effects were incorporated. In addition, in the AMOEBA+ model, the original Thole polarization model (direct component) ²⁷⁻²⁹ was improved to better capture the MP2 many-body energy, along with better combining rules for empirical van der Waals potential.³⁰ Nevertheless, the atomic charge in the AMOEBA+ model is still independent of the local geometry changes. Consequently, similar to the current AMOEBA model and other flexible water models, an artificially large equilibrium HOH angle of 108.8° was used in AMOEBA+ in order to reach the correct bending angle in the liquid phase (~106°). As mentioned above, it has been well recognized that this is attributed to the fact that the molecular charge distribution cannot properly adjust to the changing geometry, i.e. dipole derivatives are incorrect. In this work, we implement the GDCF model into AMOEBA+ potential. Different from the model proposed by Dinur and Hagler, ²⁰ only the CF along bond and angle contributions are considered. In addition, we systematically integrated the GDCF model with permanent and polarizable multipole interactions, with analytical gradients. With CF inclusion, the previous AMOEBA+ water model was reparametrized using ForceBalance toolkit ³¹ by targeting on both gas-phase QM data and liquid-phase observables, resulting in the current AMOEBA+(CF) water model.

To use a water molecule as an illustration (**Figure 1**), CF along each bond is described as a function of the deviation of bond and angle from their equilibrium values. For water, experimental angle and bond length (104.5° and 0.9572 Å) are used as the reference. The CF direction rules are kept the same as those suggested by Dinur and Hagler.²⁰ The CF on each atom is added to its permanent monopole values prior to energy and force computations. Derivation of the GDCF model in the AMOEBA+ framework, including permanent multipole and polarization energy and forces, is detailed in the **Methodologies** section and **Supporting Information (SI)**. The newly parametrized AMOEBA+(CF) water model is extensively compared with the previous AMOEBA+ and other advanced water models. Below, to clearly demonstrate the improvement due to the inclusion of GDCF, we systematically report the results on the new water model from monomer to clusters and to liquid properties.

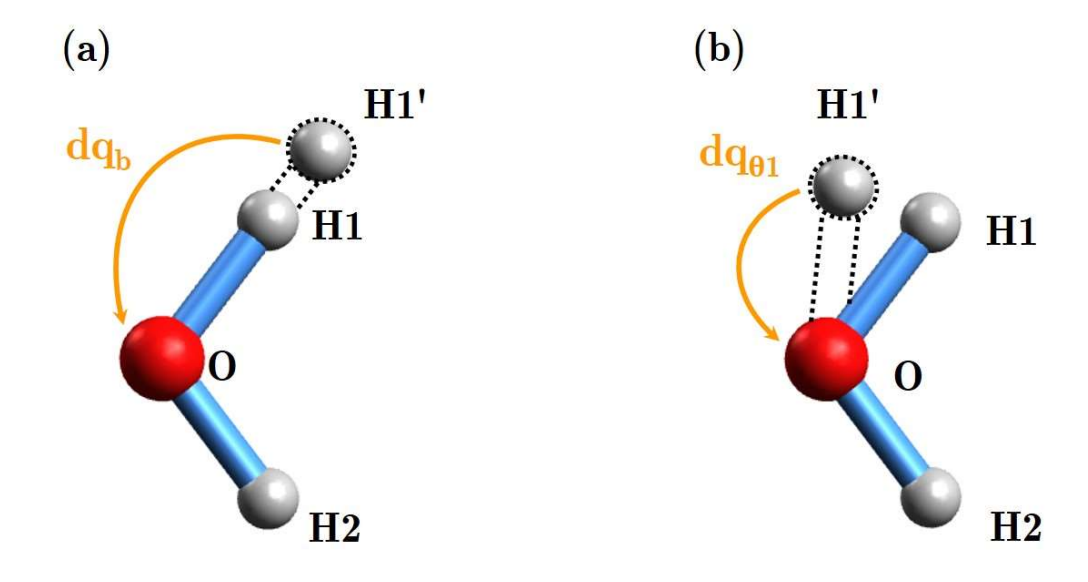


Figure 1. Schematic illustration of the GDCF model. (a) CF due to bond stretching and (b) CF due to angle bending, where dq_b and $dq_{\theta 1}$ represent the absolute charge fluxes due to bond stretching and angle bending. The direction (sign) of CF is defined in the **Methodologies** section.

Water monomer properties. As mentioned above, GDCF potentially leads to the automatic angle opening in liquid phase simulations of water. This allows us to use an angle of experimental geometry as the initial parameter. As shown in Table 1, AMOEBA+(CF) angle and bond final parameters (after cluster/liquid refinement) resemble the experimental values of an isolated water molecule. The force constants of bonded terms are adjusted slightly to better describe the experimental vibration frequencies of an isolated monomer. In addition, using the minimal-energy geometry, we show that the quality of molecular dipole, quadrupole and polarizability is significantly improved over the AMOEBA+ model, which has a compensative bigger dipole and quadrupole moments but smaller molecular polarizability. Early AMOEBA models are not shown here but they are quite similar to AMOEBA+. As expected, the final/optimal non-bonded parameters change only in small fraction comparing to those of the AMOEBA+ model (Table S1).

Table 1. The vibrational frequencies, geometrical, and moment properties of an isolated water molecule. ^a

Property		Experiment ^c	AMOEBA+ d	AMOEBA+(CF) ^e
vibrational frequency b	v_{ss}	3657	3658	3656
(cm ⁻¹)	v_{as}	3756	3757	3755
	v_b	1595	1627	1594
geometry	$b_{\mathrm{OH}}\left(\mathrm{\mathring{A}}\right)$	0.957	0.939	0.950
	$\theta_{ m HOH}$ (°)	104.52	108.82	104.54
dipole (Debye)	d_z	1.86 (1.84)	1.95	1.88

quadrupole	Q_{xx}	2.63 (2.57)	3.17	2.83
(Debye·Å)	Q_{yy}	-2.50 (-2.42)	-2.69	-2.34
	Q_{zz}	-0.13 (-0.14)	-0.48	-0.49
polarizability	α_{xx}	1.53 (1.47)	1.59	1.62
(\mathring{A}^3)	α_{yy}	1.42 (1.38)	1.21	1.24
	α_{zz}	1.47 (1.42)	1.33	1.36

^a Values in bold indicate a better consistency with the experimental data;

Water dimer properties. Both the binding energy (Eq. 1) and interaction energy (Eq. 2) were computed. The former used optimized monomers as references where keeps the monomers the same as in the dimer geometry. The dissociation energy (negative of binding energy) of the canonical hydrogen-bonding water dimer from the AMOEBA+(CF) model is 4.87 kcal/mol, which is slightly improved comparing to AMOEBA+ (4.81 kcal/mol) and in agreement with the CCSD(T)/CBS ³⁷ value of 4.98 kcal/mol. In addition, the AMOEBA+(CF) predicts intermolecular interaction energy components, including electrostatics, induction and van der Waals matching those from the SAPT2+ model (Figure S1). Besides the canonical HB dimer, the "Smith dimers" formed through different directional HBs often serve as model dimers to examine the anisotropy of water models. AMOEBA+(CF) predicts the binding energy of 10 Smith dimers extremely well with an RMSE 0.25 kcal/mol comparing to that of 0.59 kcal/mol of AMOEBA+ model. As an additional comparison, the results from the MB-UCB water model, ³⁹ which shares many similarities with the AMOEBA+ model, are also provided in Table 2.

^b v_{ss} : symmetrical stretching; v_{as} : asymmetrical stretching; v_b : bending vibration;

^c Experimental data were taken from references: vibrational frequencies,³² geometry,³² dipole,³³ quadrupole,³⁴ and polarizability;³⁵ values in parentheses are *ab initio* data taken from reference;³⁶ d Calculated with AMOEBA+ optimized monomer geometry;

^e Calculated with AMOEBA+(CF) optimized monomer geometry.

$$\Delta E_{binding} = E_{dimer}^{opt} - 2E_{monomer}^{opt} \tag{1}$$

$$\Delta E_{interaction} = E_{dimer} - E_{monomer1}^* - E_{monomer2}^* \tag{2}$$

In the above equations, superscripts *opt* means optimized geometry and * means monomer geometry kept the same as in dimer.

Table 2. Binding energies (with MP2-optimized geometry) of Smith dimers predicted by several water models comparing to CCSD(T)/CBS data. All energies are in kcal/mol.

Structure	CCSD(T)/CBS ab	AMOEBA+ ac	AMOEBA+(CF) ^a	MB-UCB d
Smith01	-4.97	-5.42 (-4.96)	-4.98	-5.15
Smith02	-4.45	-4.57 (-4.11)	-4.37	-4.78
Smith03	-4.42	-4.45 (-4.00)	-4.29	-3.86
Smith04	-4.25	-5.20 (-4.75)	-4.09	-3.11
Smith05	-4.00	-4.53 (-4.08)	-3.53	-3.68
Smith06	-3.96	-4.36 (-3.90)	-3.38	-3.21
Smith07	-3.26	-4.15 (-3.69)	-3.19	-2.93
Smith08	-1.30	-1.85 (-1.39)	-1.38	-1.15
Smith09	-3.05	-3.67 (-3.22)	-3.03	-2.99
Smith10	-2.18	-2.79 (-2.34)	-2.27	-2.07
	RMSE	0.59 (0.28)	0.25	0.51

a. BEs using MP2-optimized geometry for dimer and monomer; 31, 38

Larger water clusters. We demonstrate here that AMOEBA+(CF) model is capable of accurately predicting *both binding energy (BE) and interaction energy (IE)* for large water clusters from trimer to 17-mers comparing to available CCSD(T)/CBS data. Here the BEs of water models were

b. CCSD(T)/CBS values were taken from reference;⁴⁰

c. Values in parentheses are BEs using MP2-optimized dimer and experimental monomer. These values were reported in the previous AMOEBA+ publication;²⁶

d. These values were taken from reference. ³⁹

calculated from FF-optimized geometry while the CCSD(T)/CBS used the MP2-optimized geometry. The IEs were calculated using the MP2-optimized cluster geometry for both the QM and FFs. As seen from **Figure 2a-c** for BEs for clusters from trimer to 17-mers, MB-UCB and AMOEBA+ give overall RMSEs of 2.95 and 1.89 kcal·mol⁻¹ respectively. AMOEBA+(CF) model remarkably reduces the error to 0.67 kcal/mol (**Table S2**). For the IEs of tetra-, penta- and hexamer isomers, the AMOEBA+ model gives an RMSE of 1.74 kcal/mol and AMOEBA+(CF) significantly reduces the error to 0.36 kcal/mol, which is slightly better than MB-pol water model (0.39 kcal/mol) (**Table S3**). It is worth mentioning that the MB-pol model was explicitly fitted on the IEs of water clusters⁴¹ while only the BEs were included as the targets in AMOEBA+(CF) parameterization (in addition to selected liquid properties). These results further indicate the importance of a correct monomer geometry for a flexible water model to accurately capture the complicated energy surfaces of water clusters.

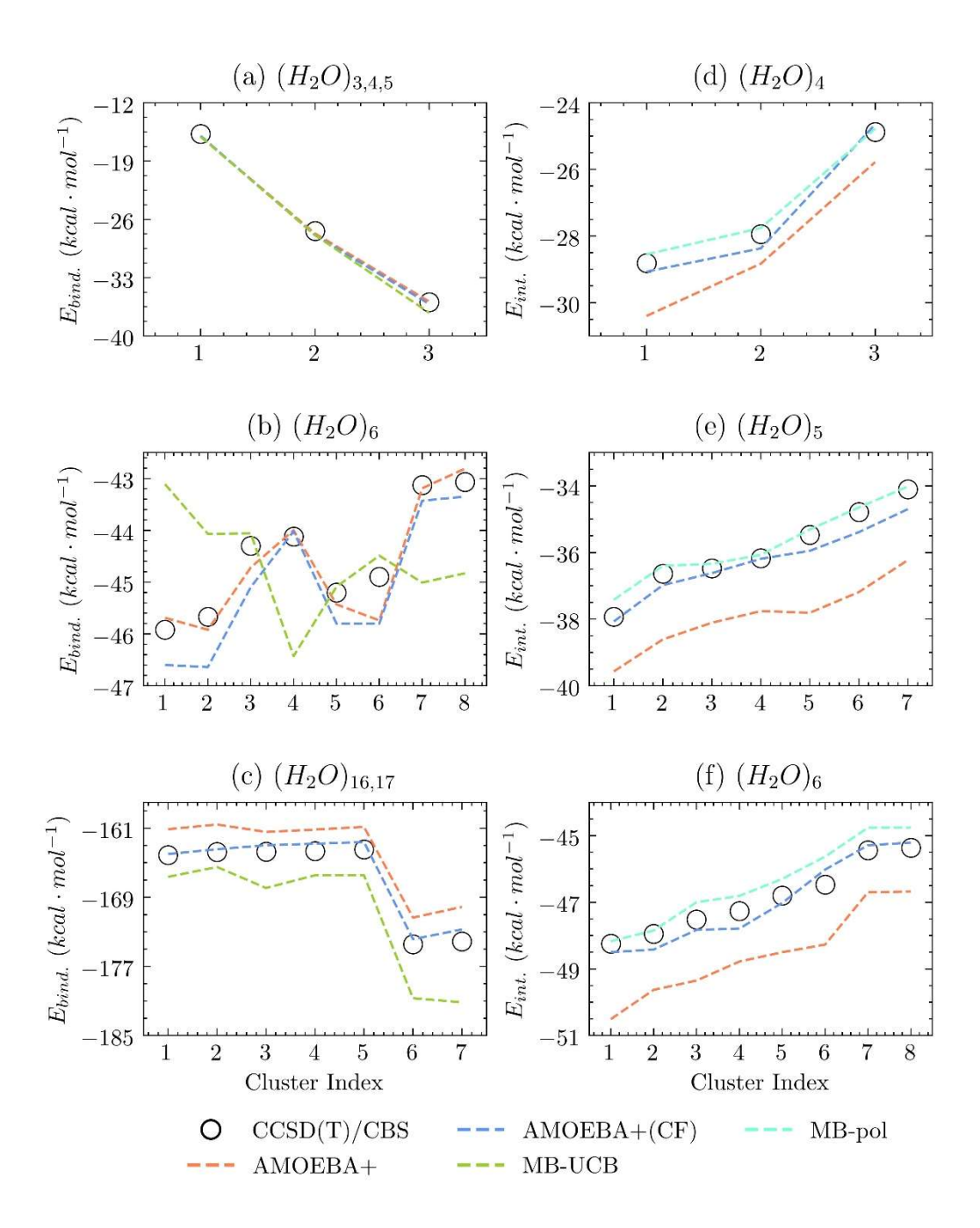


Figure 2. Binding energy and interaction energy computed with water models compared with available *ab initio* CCSD(T)/CBS data. **(a)-(c)**: BEs of water trimer to 17-mers and **(d)-(f)**: IEs of water tetramer, pentamer and hexamer conformers. The BEs from MB-UCB ³⁹ and IEs from MB-pol ⁴¹ water models are provided for comparison. The numerical data, cluster indices and references are provided in **Table S2** and **Table S3**.

Liquid properties. As shown above, the addition of CF to AMOEBA+ significantly improves its ability to describe the structural and energetic properties of gas-phase water clusters. Here we examine the performance of AMOEBA+(CF) in liquid. Overall, AMOEBA+(CF) model maintains the quality of the AMOEBA+ model on predicting the average thermodynamic, structural and dynamic properties over a broad range of temperatures (Figure 3). For six thermodynamic properties included in the parametrization targets, density (Figure 3a), enthalpy of vaporization (Figure 3b), thermal expansion coefficient (Figure 3c) and isothermal compressibility (Figure 3e), AMOEBA+(CF) captures the experimental properties as well as the previous AMOEBA+ model. AMOEBA+(CF) liquid water density at room temperature is 997.4±0.1 kg/m³, almost exactly the same as experimental measurement (997.0 kg·m⁻³), when a larger box of 60 Å³ and a van der Waals cutoff of 12 Å are used. At 298 K, AMOEBA+(CF) is slightly worse than the AMOEBA+ model by 1.0 cal/mol/K on predicting the isobaric heat capacity (Figure 3f), which is known to be difficult for flexible classical water models due to nuclear quantum effect. 42 AMOEBA+(CF) notably improves the agreement with experiment for the static dielectric constant in the whole temperature range comparing to AMOEBA+ (Figure 3d). This can be attributed to a better quality of electrostatics, including CF-augmented-multipole moments and polarizability of the AMOEBA+(CF) model than AMOEBA+ (Table 1). At ambient conditions (298K, 1 atm), AMOEBA+(CF) results in a static dielectric constant of 78.8±3.1, in excellent agreement with the experiment (78.4). The liquid properties which were not included in the parametrization targets are also well reproduced by AMOEBA+(CF) model, as shown in Figure 3g and Figure S2 (SI) for the radial distribution function at ambient conditions and Figure 3h for the self-diffusion constant at a series of temperatures (also Figure S3 and Table S4). The average O-H bond length and H-O-H angle in liquid by AMOEBA+(CF) are 0.96 Å and 105.5°±4.7°, while experimental values are 0.97 Å and

 $106.1^{\circ}\pm1.8^{\circ}$. Coincidently, AMOEBA+(CF) liquid HOH angle is consistent with the value of *ab initio* MD simulations (105.5°). By contrast, AMOEBA+ gives an appropriate average angle ($106.3^{\circ}\pm4.7^{\circ}$) but shorter bond length (0.95 Å) in liquid (also in cluster as shown by Hughes *et al.*⁴⁴). It is worth noting that although both water models correctly predict the average angle, as mentioned above, AMOEBA+ angle is originated from an artificially large equilibrium angle parameter (108.8°) while the AMOEBA+(CF) water automatically expanded from 104.5° in isolation to 105.5° in liquid due to CF. The average amount of charges transferred for a water molecule due to the geometrical deviation is only -0.0031 *e* on the oxygen atom, of which -0.0040 *e* is contributed from angle bending, +0.0004 *e* from symmetrical bond stretching and +0.0005 *e* from asymmetrical bond stretching.

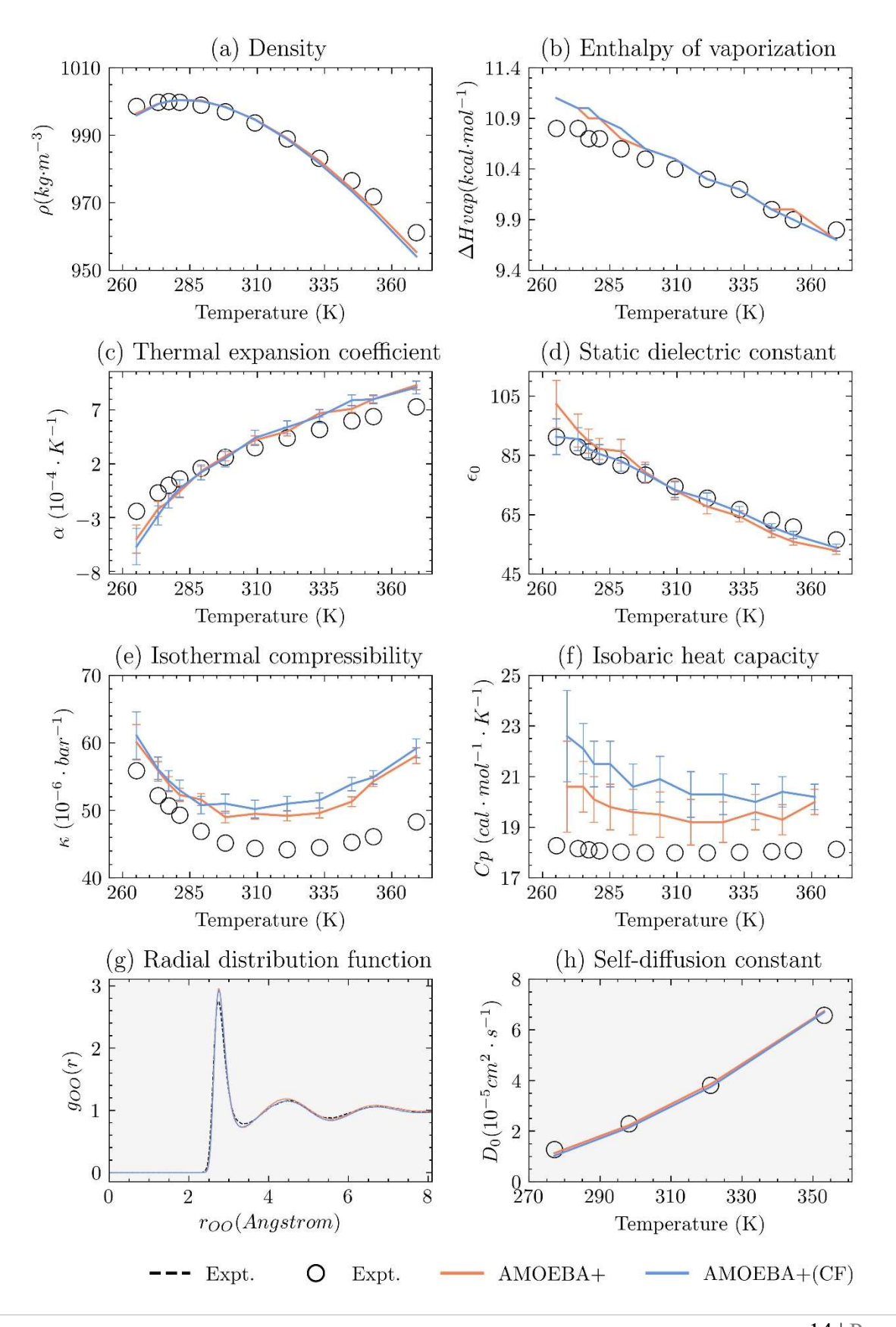


Figure 3. Liquid properties of water at a broad range of temperatures and 1 atm pressure. Properties in (a)-(f) were included in the ForceBalance optimization while (g)-(h) were not used in parametrization. Error bars are also plotted if they are notable. The radial distribution function of oxygen-hydrogen and hydrogen-hydrogen pairs are provided in **Figure S2**.

Infrared spectra of liquid water. It has been shown by the SDFF water model that charge flux is necessary to describe the dipole surface and vibrational spectra. 15 It is also observed that iAMOEBA fails to predict the correct relative intensity of experimental infrared (IR) spectra. ⁴⁵ To investigate the impact of CF on the liquid IR spectra, we examined several AMOEBA-based water models either with or without CF. IR spectra were obtained within linear response theory through Fourier transforms of time correlation of net dipole (simulation details in SI). To compare with experimental IR spectra, corrections accounting for quantum effects were added to the calculated IR intensity by using a previously suggested approach. ⁴⁶ Figure 4 clearly indicates that without CF implementation, both AMOEBA14 and AMOEBA+ models predict a higher bending peak (~1600 cm⁻¹) than the libration peak (~480 cm⁻¹), which was similarly observed for the AMOEBA03 water (Figure S4) and iAMOEBA models. 45 By contrast, AMOEBA+(CF) reduces the height of the bending peak and results in correct relative intensity comparing to the experiment. In the OH stretching region, it is seen that the stretching is shifted to low frequencies (blue shift) from 3755 cm⁻¹ (asymmetric) and 3656 cm⁻¹ (symmetric) of an isolated water molecule (**Table 1**) to ~3550 cm⁻¹ (Figure S4). This blue shift magnitude is insufficient comparing to experiment, which can be attributed to the lack of the explicit treatment of the nuclear quantum effect in this high-frequency region for classical models. 47-48 With an adjusted bond stretching force constant, AMOEBA+(CF) model is able to predict the correct peak position (~3400 cm⁻¹). Additionally, it is clear that a "stiffer" bond stretching force constant also helps to prevent the peak splitting observed in AMOEBA+(CF) using gas-phase force constant, as well as other models (**Figure 4** and **Figure S4**). Thus this modified model is suggested for vibrational spectroscopy simulation in water. This modification on the bond stretching force constant has no effect on average liquid thermodynamic or dynamic properties we have computed.

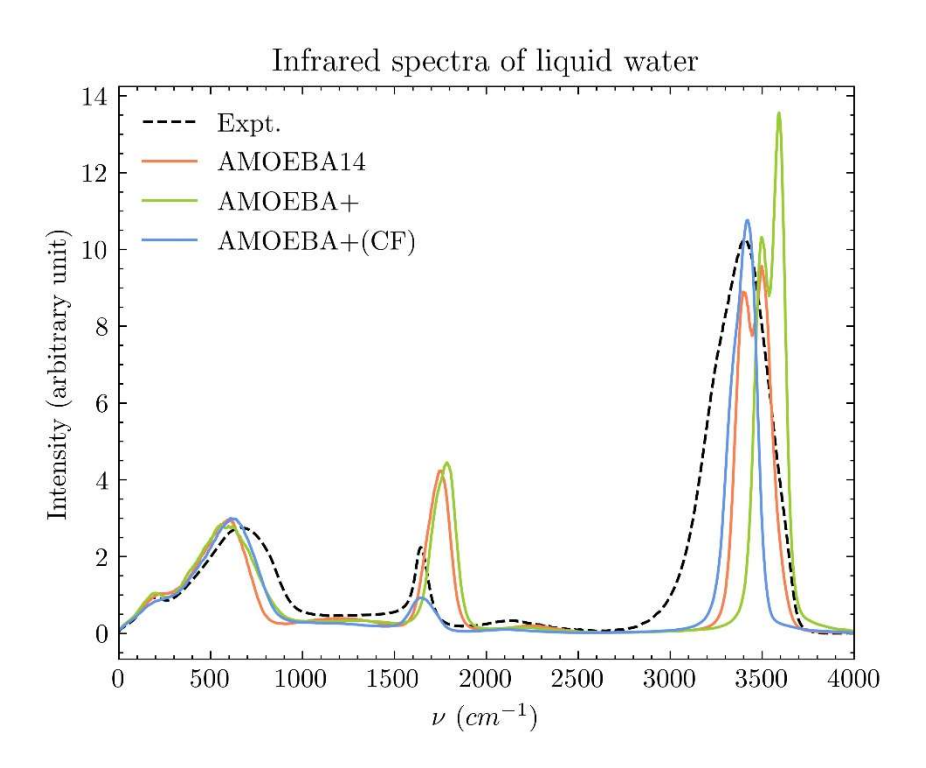


Figure 4. IR spectra of liquid water calculated with water models with/without charge flux and compared to the experiment. Experimental data were taken from the literature of ambient conditions (298 K and 1 atm).⁴⁹ Quantum corrections were added to each calculated spectra using the same approach suggested by a previous study.⁴⁶ More simulation details are provided in **SI**.

Ice properties. Three crystal forms of ice, Ih, Ic and II, were simulated at 1 *atm* pressure and experimental temperatures by employing AMOEBA+ and AMOEBA+(CF) water models. The

computational details are provided in SI and the results are summarized in Table S11 and S12. The average density simulated by our models agree reasonably well with experiment within ~2% for Ih, ~4% for Ic and ~6% for ice II (**Table S11**), which can be attributed to two factors: (1) the lack of nuclear quantum effect, which normally leads to a reduction of the simulated density and (2) the exclusion of solid-phase properties in our parametrization. As shown in Table S12, AMOEBA+(CF) model shows the reasonable capability to predict other properties of ice Ih without explicitly parametrizing to ice data. For example, simulated enthalpy of sublimation for ice Ih at 269 K and 1 atm is -12.13 kcal/mol, which excellently agrees with experiment (-12.20 kcal/mol). 50 By contrast, TTM-family models over-predict enthalpy of sublimation of ice Ih, with TTM4-F being -14.40 kcal/mol and TTM2-F being 13.39 kcal/mol.⁵¹ The average intermolecular OO distance (2.73 Å) is ~1% shorter than experimental value (2.76 Å), which is consistent with slightly higher simulated density. The intramolecular OH distance (0.97 Å) is in agreement with experiment (0.98 Å).⁵² Experimental value of the HOH angle is commonly referenced as ideal tetrahedral angle of 109.5°. A trend of HOH angle expansion (gas < liquid < ice) consistent to experiment is observed for the AMOEBA+(CF) model in three phases while the AMOEBA+ model gives the opposite trend as gas > liquid > ice.

In summary, we implemented the GDCF model into the multipole-based polarizable AMOEBA+ potential. The GDCF model was originally proposed by Dinur and Hagler and examined on small organic molecules within the point charge electrostatic framework.²⁰ In this work, we integrated the GDCF model with atomic multipole electrostatics (with permanent multipoles up to quadrupole) and many-body atomic dipole polarization in the AMOEBA+ framework. The energy and

force expressions due to the inclusion of GDCF were derived. We examined the impact of GDCF by updating the AMOEBA+ water model. Our results indicate that GDCF allows the use of appropriate equilibrium angle and bond length for an isolated water molecule which will spontaneously adjust to the correct values in liquid. The correct monomer geometry and GDCF lead to noticeable improvements in both the binding energy and the interaction energy of water clusters. Finally, AMOEBA+(CF) water model shows excellent liquid properties, along with improved IR spectra in terms of capturing the relative intensity of bending and libration peaks.

The preliminary implementation of AMOEBA+(CF) was finished on our developing version of Tinker (CPU) and Tinker-OpenMM (GPU). MD simulations under NVE ensemble were carried out on both CPU and GPU codes to evaluate the energy conservation of the AMOEBA+(CF) model (simulation details in SI). To take advantage of the double precision of Tinker CPU code, simulation using a very tight induced dipole convergence (polar-eps 10⁻¹² D) with the iterative SCF method leads to only -0.01 kcal/mol/ns of total energy drift (out of ~ -3800 kcal/mol) (Figure S5a). Alternatively, simulation with the "OPT4" extrapolated polarization scheme⁵³ on CPU gives a total energy drift of -0.03 kcal/mol/ns (Figure S5b). As expected, simulations on Tinker-OpenMM GPU (mixed precision) give a greater total energy drift of -0.2 kcal/mol/ns (**Figure S5c**) and +0.1 kcal/mol/ns (Figure S5d) for SCF (polar-eps 10⁻⁶ D due to single precision) and "OPT4" scheme respectively. These results indicate the excellent energy conservation of our implementation. Besides, it is shown that a negligible additional cost (less than 1%) arises from the GDCF algorithms. Further code implementation and optimization in the latest version of Tinker, 54 Tinker-OpenMM⁵⁵ and Tinker-HP⁵⁶ are ongoing, as well as the parametrization of AMOEBA+(CF) for a wide range of molecular systems.

METHODOLOGIES

Here we briefly describe the theoretical methodologies of CF implementation. AMOEBA+ potential adopts atomic multipoles to represent atomic charge distributions, with short-range penetration effect. Multipole moments on atom i can be expressed as

$$M_i = [q, \mu_x, \mu_y, \mu_z, \Theta_{xx}, \dots]$$

$$\tag{4}$$

To implement the GDCF model, we followed the algorithms proposed by Dinur and Hagler²⁰ by only including the bond and angle contributions. For a pair of bonded atoms a and b, CFs on atom a and b due to bond stretching are expressed as

$$dq_a = -dq_b = j_b(r_{ab} - r_{ab}^0) (5)$$

where r_{ab} and r_{ab}^0 are the actual and equilibrium bond lengths; j_b is the determining parameter specific to this bond. The CF direction rule is kept the same as previous work. ²⁰ Briefly, – dq is added to the (1) atom with a bigger atomic number; (2) atom with more connections if rule (1) is not applicable; (3) atom with more connected hydrogen atoms if both (1) and (2) are not applicable. For an angle $\angle abc$, the CFs due to angle bending are expressed as

$$dq_a = j_{\theta 1}(\theta - \theta_0) + j'_{h1}(r_{hc} - r_{hc}^0)$$
(6)

$$dq_c = j_{\theta 2}(\theta - \theta_0) + j'_{h2}(r_{ab} - r_{ab}^0)$$
(7)

$$dq_b = -(dq_a + dq_c) (8)$$

where θ and θ_0 are actual and equilibrium angle values; the second terms on the right side is due to asymmetric stretching, in which case change of r_{bc} also affects atom $a.\ j_{\theta 1},\ j_{\theta 2},\ j'_{b1}$ and j'_{b2} are

CF parameters determined by the chemistry (atom types). The initial CF parameters of water were derived by fitting to the molecular dipole surface using MP2/aug-cc-pvtz level of theory. In Force-Balance optimization, only the j_{θ} is allowed to be further optimized as we found it is more sensitive to the HOH angle than the bond-related CF parameters. For organic molecules and peptides, density functional theory may be applied to calculate the dipole surface, as also suggested by other researchers. ¹⁸⁻¹⁹

With the CF dq_i for atomic site i determined for a given geometry, the monopole in AMOEBA+ multipole moments then is replaced by $q + dq_i$. The modified multipole is then

$$M_i' = [q + dq_i, \mu_x, \mu_y, \mu_z, \Theta_{xx}, \dots]$$

$$(9)$$

With the above multipoles, permanent electrostatics of AMOEBA+ is calculated as

$$E_{ele} = \sum_{i,j} M_i' T^{damped} M_j' \tag{10}$$

wherein the AMOEBA+ potential, the multipole-multipole interaction T matrix is damped to account for the charge penetration effect. ²⁵⁻²⁶ Induced dipole and polarization energy are calculated in the same manner as current AMOEBA+ model with the updated multipoles M'.

In order to use the GDCF model in MD simulations, one needs the gradient of the potential energy *w.r.t.* atom coordinate. We found that the final form of the electrostatic and polarization forces can be expressed in the following formula

$$F_{i,\alpha}(CF) = F_{i,\alpha} + F'_{i,\alpha} \tag{11}$$

 $(\alpha = x, y, z)$

The first term on the right side stands for the usual AMOEBA+ electrostatics and polarization

terms with CF-updated charges. The second chain-rule term arises from CF which explicitly de-

pends on the internal bonds and angles. In SI, we show that F' can be calculated using the accu-

mulated potential on each atom (V_i) and the derivative of CF w.r.t. coordinates $\left(\frac{\partial dq_i}{\partial \alpha}\right)$. The V_i term

in AMOEBA+ framework is contributed from permanent multipoles (charge, dipole, and quadru-

pole) and induced dipole. These expressions of V_i are already calculated in the AMOEBA+ poten-

tial.²⁵⁻²⁶ In addition, since charges in our model now depends on the atomic coordinates, extra force

contribution to Ewald self-energy appears (see detailed derivation in SI).

ASSOCIATED CONTENT

Code Availability

All code is available in the publically accessible TinkerTools Github site as Tinker/AMOEBA+CF

and Tinker-OpenMM/AMOEBA+CF branch.

Supporting Information

Additional methodologies, figures, tables, numerical results and references (PDF).

AUTHOR INFORMATION

Corresponding Author

Email: pren@utexas.edu

ACKNOWLEDGMENT

21 | Page

The authors are grateful for support by the Robert A. Welch Foundation (F-1691), National Institutes of Health (R01GM106137 and R01GM114237), the Cancer Prevention and Research Institute of Texas (RP160657), National Science Foundation (CHE-1856173) and European Research Council (ERC) under the European Union's Horizon 2020 research and innovation program (grant agreement No 810367), project EMC2.

REFERENCES

- 1. Hagler, A. T., Force field development phase II: Relaxation of physics-based criteria... or inclusion of more rigorous physics into the representation of molecular energetics. *J. Comput. Aided Mol. Des.* **2019**, *33* (2), 205.
- 2. Lemkul, J. A.; Huang, J.; Roux, B.; MacKerell, A. D., Jr., An Empirical Polarizable Force Field Based on the Classical Drude Oscillator Model: Development History and Recent Applications. *Chem Rev* **2016**, *116* (9), 4983.
- 3. Jing, Z.; Liu, C.; Cheng, S. Y.; Qi, R.; Walker, B. D.; Piquemal, J.-P.; Ren, P., Polarizable Force Fields for Biomolecular Simulations: Recent Advances and Applications. *Annu. Rev. Biophys* **2019**.
- 4. Patel, S.; Brooks, C. L., Fluctuating charge force fields: recent developments and applications from small molecules to macromolecular biological systems. *Molecular Simulation* **2006**, *32* (3-4), 231.
- 5. Patel, S.; Brooks III, C. L., CHARMM fluctuating charge force field for proteins: I parameterization and application to bulk organic liquid simulations. *J Comput Chem* **2004**, *25* (1), 1.
- 6. Patel, S.; Mackerell Jr., A. D.; Brooks III, C. L., CHARMM fluctuating charge force field for proteins: II Protein/solvent properties from molecular dynamics simulations using a nonadditive electrostatic model. *J Comput Chem* **2004**, *25* (12), 1504.
- 7. Poier, P. P.; Jensen, F., Describing Molecular Polarizability by a Bond Capacity Model. *J. Chem. Theory Comput.* **2019**, *15* (5), 3093.
- 8. Benedict, W. S.; Gailar, N.; Plyler, E. K., Rotation-Vibration Spectra of Deuterated Water Vapor. *J. Chem. Phys.* **1956**, *24* (6), 1139.
- 9. Ichikawa, K.; Kameda, Y.; Yamaguchi, T.; Wakita, H.; Misawa, M., Neutron-diffraction investigation of the intramolecular structure of a water molecule in the liquid phase at high temperatures. *Mol. Phys.* **1991**, *73* (1), 79.
- 10. Kuhs, W. F.; Lehmann, M. S., The structure of the ice Ih by neutron diffraction. *J. Phys. Chem.* **1983**, 87 (21), 4312.
- 11. Fanourgakis, G. S.; Xantheas, S. S., The bend angle of water in ice Ih and liquid water: The significance of implementing the nonlinear monomer dipole moment surface in classical interaction potentials. *J. Chem. Phys.* **2006**, *124* (17), 174504.
- 12. Dinur, U., "Flexible" water molecules in external electrostatic potentials. *J. Phys. Chem.* **1990,** *94* (15), 5669.

- 13. Palmo, K.; Mannfors, B.; Mirkin, N. G.; Krimm, S., Inclusion of charge and polarizability fluxes provides needed physical accuracy in molecular mechanics force fields. *Chem Phys Lett* **2006**, *429* (4), 628.
- 14. Palmo, K.; Mannfors, B.; Krimm, S., Balanced charge treatment of intramolecular electrostatic interactions in molecular mechanics energy functions. *Chem Phys Lett* **2003**, *369* (3), 367.
- 15. Mannfors, B.; Palmo, K.; Krimm, S., Spectroscopically Determined Force Field for Water Dimer: Physically Enhanced Treatment of Hydrogen Bonding in Molecular Mechanics Energy Functions. *J Phys Chem A* **2008**, *112* (49), 12667.
- 16. Burnham, C. J.; Xantheas, S. S., Development of transferable interaction models for water. IV. A flexible, all-atom polarizable potential (TTM2-F) based on geometry dependent charges derived from an ab initio monomer dipole moment surface. *J. Chem. Phys.* **2002**, *116* (12), 5115.
- 17. Fanourgakis, G. S.; Xantheas, S. S., Development of transferable interaction potentials for water. V. Extension of the flexible, polarizable, Thole-type model potential (TTM3-F, v. 3.0) to describe the vibrational spectra of water clusters and liquid water. *J. Chem. Phys.* **2008**, *128* (7), 074506.
- 18. Sedghamiz, E.; Nagy, B.; Jensen, F., Probing the Importance of Charge Flux in Force Field Modeling. *J. Chem. Theory Comput.* **2017**, *13* (8), 3715.
- 19. Sedghamiz, E.; Ghalami, F., Evaluating the Effects of Geometry and Charge Flux in Force Field Modeling. *J Phys Chem A* **2018**, *122* (19), 4647.
- 20. Dinur, U.; Hagler, A. T., Geometry-dependent atomic charges: Methodology and application to alkanes, aldehydes, ketones, and amides. *J Comput Chem* **1995**, *16* (2), 154.
- 21. Ren, P. Y.; Ponder, J. W., Polarizable atomic multipole water model for molecular mechanics simulation. *J. Phys. Chem. B* **2003**, *107* (24), 5933.
- 22. Shi, Y.; Xia, Z.; Zhang, J.; Best, R.; Wu, C.; Ponder, J. W.; Ren, P., Polarizable Atomic Multipole-Based AMOEBA Force Field for Proteins. *J. Chem. Theory Comput.* **2013**, *9* (9), 4046.
- 23. Zhang, C.; Bell, D.; Harger, M.; Ren, P., Polarizable Multipole-Based Force Field for Aromatic Molecules and Nucleobases. *J. Chem. Theory Comput.* **2017**, *13* (2), 666.
- 24. Ponder, J. W.; Wu, C.; Ren, P.; Pande, V. S.; Chodera, J. D.; Schnieders, M. J.; Haque, I.; Mobley, D. L.; Lambrecht, D. S.; DiStasio, R. A., Jr.; Head-Gordon, M.; Clark, G. N.; Johnson, M. E.; Head-Gordon, T., Current status of the AMOEBA polarizable force field. *J Phys Chem B* **2010**, *114* (8), 2549.
- 25. Rackers, J. A.; Wang, Q.; Liu, C.; Piquemal, J.-P.; Ren, P.; Ponder, J. W., An optimized charge penetration model for use with the AMOEBA force field. *Phys. Chem. Chem. Phys.* **2017**, 19 (1), 276.
- 26. Liu, C.; Piquemal, J.-P.; Ren, P., AMOEBA+ Classical Potential for Modeling Molecular Interactions. *J. Chem. Theory Comput.* **2019**, *15* (7), 4122.
- 27. Liu, C.; Qi, R.; Wang, Q.; Piquemal, J. P.; Ren, P., Capturing Many-Body Interactions with Classical Dipole Induction Models. *J Chem Theory Comput* **2017**, *13* (6), 2751.
- 28. Thole, B. T., Molecular Polarizabilities Calculated with a Modified Dipole Interaction. *Chem Phys* **1981**, *59* (3), 341.
- 29. van Duijnen, P. T.; Swart, M., Molecular and Atomic Polarizabilities: Thole's Model Revisited. *J Phys Chem A* **1998**, *102* (14), 2399.
- 30. Qi, R.; Wang, Q.; Ren, P., General van der Waals potential for common organic molecules. *Bioorg Med Chem* **2016**, *24* (20), 4911.

- 31. Wang, L. P.; Martinez, T. J.; Pande, V. S., Building Force Fields: An Automatic, Systematic, and Reproducible Approach. *J Phys Chem Lett* **2014**, *5* (11), 1885.
- 32. Ben-Naim, A., Molecular Theory of Water and Aqueous Solutions. World Scientific: 2011.
- 33. Clough, S. A.; Beers, Y.; Klein, G. P.; Rothman, L. S., Dipole moment of water from Stark measurements of H2O, HDO, and D2O. *J. Chem. Phys.* **1973**, *59* (5), 2254.
- 34. Verhoeven, J.; Dymanus, A., Magnetic Properties and Molecular Quadrupole Tensor of the Water Molecule by Beam-Maser Zeeman Spectroscopy. *J. Chem. Phys.* **1970**, *52* (6), 3222.
- 35. Murphy, W. F., The Rayleigh depolarization ratio and rotational Raman spectrum of water vapor and the polarizability components for the water molecule. *J. Chem. Phys.* **1977**, *67* (12), 5877.
- 36. Maroulis, G., Hyperpolarizability of H2O revisited: accurate estimate of the basis set limit and the size of electron correlation effects. *Chem Phys Lett* **1998**, *289* (3-4), 403.
- 37. Tschumper, G. S.; Leininger, M. L.; Hoffman, B. C.; Valeev, E. F.; Schaefer, H. F.; Quack, M., Anchoring the water dimer potential energy surface with explicitly correlated computations and focal point analyses. *J. Chem. Phys.* **2002**, *116* (2), 690.
- 38. Smith, B. J.; Swanton, D. J.; Pople, J. A.; III, H. F. S.; Radom, L., Transition structures for the interchange of hydrogen atoms within the water dimer. *J. Chem. Phys.* **1990**, *92* (2), 1240.
- 39. Das, A. K.; Urban, L.; Leven, I.; Loipersberger, M.; Aldossary, A.; Head-Gordon, M.; Head-Gordon, T., Development of an Advanced Force Field for Water Using Variational Energy Decomposition Analysis. *J. Chem. Theory Comput.* **2019**, *15* (9), 5001.
- 40. Laury, M. L.; Wang, L. P.; Pande, V. S.; Head-Gordon, T.; Ponder, J. W., Revised Parameters for the AMOEBA Polarizable Atomic Multipole Water Model. *J Phys Chem B* **2015**, *119* (29), 9423.
- 41. Reddy, S. K.; Straight, S. C.; Bajaj, P.; Pham, C. H.; Riera, M.; Moberg, D. R.; Morales, M. A.; Knight, C.; Götz, A. W.; Paesani, F., On the accuracy of the MB-pol many-body potential for water: Interaction energies, vibrational frequencies, and classical thermodynamic and dynamical properties from clusters to liquid water and ice. *J. Chem. Phys.* **2016**, *145* (19), 194504.
- 42. Vega, C.; Conde, M. M.; McBride, C.; Abascal, J. L. F.; Noya, E. G.; Ramirez, R.; Sesé, L. M., Heat capacity of water: A signature of nuclear quantum effects. *J. Chem. Phys.* **2010**, *132* (4), 046101.
- 43. Silvestrelli, P. L.; Parrinello, M., Structural, electronic, and bonding properties of liquid water from first principles. *J. Chem. Phys.* **1999**, *111* (8), 3572.
- 44. Hughes, Z. E.; Ren, E.; Thacker, J. C. R.; Symons, B. C. B.; Silva, A. F.; Popelier, P. L. A., A FFLUX Water Model: Flexible, Polarizable and with a Multipolar Description of Electrostatics. *J Comput Chem* **2019**, *doi:* 10.1002/jcc.26111.
- 45. Wang, L. P.; Head-Gordon, T.; Ponder, J. W.; Ren, P.; Chodera, J. D.; Eastman, P. K.; Martinez, T. J.; Pande, V. S., Systematic improvement of a classical molecular model of water. *J Phys Chem B* **2013**, *117* (34), 9956.
- 46. Gaigeot, M.-P.; Sprik, M., Ab Initio Molecular Dynamics Computation of the Infrared Spectrum of Aqueous Uracil. *J. Phys. Chem. B* **2003**, *107* (38), 10344.
- 47. Medders, G. R.; Paesani, F., Infrared and Raman Spectroscopy of Liquid Water through "First-Principles" Many-Body Molecular Dynamics. *J. Chem. Theory Comput.* **2015**, *11* (3), 1145.
- 48. Kapil, V.; VandeVondele, J.; Ceriotti, M., Accurate molecular dynamics and nuclear quantum effects at low cost by multiple steps in real and imaginary time: Using density functional theory to accelerate wavefunction methods. *J. Chem. Phys.* **2016**, *144* (5), 054111.

- 49. Maréchal, Y., The molecular structure of liquid water delivered by absorption spectroscopy in the whole IR region completed with thermodynamics data. *J. Mol. Struct.* **2011**, *1004* (1), 146.
- 50. Murphy, D. M.; Koop, T., Review of the vapour pressures of ice and supercooled water for atmospheric applications. *Quarterly Journal of the Royal Meteorological Society* **2005**, *131* (608), 1539.
- 51. Burnham, C. J.; Anick, D. J.; Mankoo, P. K.; Reiter, G. F., The vibrational proton potential in bulk liquid water and ice. *J. Chem. Phys.* **2008**, *128* (15), 154519.
- 52. Floriano, M. A.; Klug, D. D.; Whalley, E.; Svensson, E. C.; Sears, V. F.; Hallman, E. D., Direct determination of the intramolecular O–D distance in ice Ih and Ic by neutron diffraction. *Nature* **1987**, *329* (6142), 821.
- 53. Simmonett, A. C.; IV, F. C. P.; Ponder, J. W.; Brooks, B. R., An empirical extrapolation scheme for efficient treatment of induced dipoles. *J. Chem. Phys.* **2016**, *145* (16), 164101.
- 54. Rackers, J. A.; Wang, Z.; Lu, C.; Laury, M. L.; Lagardère, L.; Schnieders, M. J.; Piquemal, J. P.; Ren, P.; Ponder, J. W., Tinker 8: Software Tools for Molecular Design. *J Chem Theory Comput* **2018**, *14* (10), 5273.
- 55. Eastman, P.; Swails, J.; Chodera, J. D.; McGibbon, R. T.; Zhao, Y.; Beauchamp, K. A.; Wang, L. P.; Simmonett, A. C.; Harrigan, M. P.; Stern, C. D.; Wiewiora, R. P.; Brooks, B. R.; Pande, V. S., OpenMM 7: Rapid development of high performance algorithms for molecular dynamics. *PLoS Comput Biol* **2017**, *13* (7), e1005659.
- 56. Lagardère, L.; Jolly, L. H.; Lipparini, F.; Aviat, F.; Stamm, B.; Jing, Z. F.; Harger, M.; Torabifard, H.; Cisneros, G. A.; Schnieders, M. J.; Gresh, N.; Maday, Y.; Ren, P. Y.; Ponder, J. W.; Piquemal, J. P., Tinker-HP: a massively parallel molecular dynamics package for multiscale simulations of large complex systems with advanced point dipole polarizable force fields. *Chem Sci* **2018**, *9* (4), 956.

Implementation of Geometry Dependent Charge Flux into Polarizable AMOEBA+ Potential

Chengwen Liu, † Jean-Philip Piquemal, †,‡,§ and Pengyu Ren †,*

[†] Department of Biomedical Engineering, The University of Texas at Austin, Austin, TX 78712, USA [‡] Laboratoire de Chimie Théorique, Sorbonne Université, UMR7616 CNRS, Paris, France [§] Institut Universitaire de France, 75005, Paris, France

Contents

I. Derivation of chain rule terms due to charge flux	3
A. Force expression of two atoms in a bond	4
B. Force expressions of three atoms in an angle	5
C. Ewald self-energy force	6
II. Computational details	7
A. Liquid simulation in ForceBalance parametrization	7
B. Self-diffusion constant simulation.	8
C. Infrared spectra liquid simulation	8
D. Ice simulation	8
E. Liquid NVE simulation	9
III. Supplementary Figures	10
Figure S1. The intermolecular interaction energy of hydrogen-bonding dimer	10
Figure S2. Radial distribution functions at ambient conditions.	11
Figure S3. The self-diffusion constant of different temperatures and box sizes	12
Figure S4. IR spectra of liquid water calculated by various models compared to experiment	13
Figure S5. Energy-time plot of NVE simulations to demonstrate the energy conservation	14
IV. Supplementary Tables	15
Table S1. Optimal parameters of AMOEBA+ and AMOEBA+(CF) water models	15
Table S2. The binding energy of water trimer to 17-mers.	16
Table S3. The interaction energy of water tetramer, pentamer and hexamer conformers	17
Table S4 . Size-corrected self-diffusion constant D ₀ at four temperatures and 1 atm	18
Table S5 . Liquid density at a broad range of temperatures from 265 to 369 K and 1 atm	19
Table S6. Enthalpy of vaporization at temperatures from 265 to 369 K and 1 atm.	20
Table S7. Thermal expansion coefficient at temperatures from 265 to 369 K and 1 atm	21
Table S8. Isothermal compressibility at temperatures from 265 to 369 K and 1 atm	22
Table S9. Isobaric heat capacity at temperatures from 265 to 369 K and 1 atm	23
Table S10. Static dielectric constant at temperatures from 265 to 369 K and 1 atm	24
Table S11. Density of three forms of ice under 1 atm pressure and indicated temperatures	25
Table S12. Simulated geometrical and energetic properties for ice Ih at 269 K and 1 atm	26

I. Derivation of chain rule terms due to charge flux

Here we derive the general form of the force expression due to the inclusion of geometry dependent charge flux (GDCF). For clarity purposes, we start from charge-charge electrostatic interaction without GDCF. The interaction energy between atom i and j is expressed as

$$U_{ij} = \frac{q_i q_j}{r_{ij}} \tag{S1}$$

Note that atom i and j are not involved in an angle or bond (i.e., 1-4 connection and beyond). Force on atom i is expressed as

$$F_{i,\alpha} = -\frac{\partial U_{ij}}{\partial \alpha_i} = -q_i q_j \frac{(\alpha_i - \alpha_j)}{r_{ij}^3}$$

$$(\alpha = x, y, z)$$
(S2)

where $\alpha = x, y, z$ are Einstein convention and hereafter we use this convention by default. After obtaining the charge flux due to geometrical derivations from the reference values, the interaction between two atoms can be written as

$$U'_{ij} = \frac{q'_i q'_j}{r_{ij}} = \frac{(q_i + dq_i)(q_j + dq_j)}{r_{ij}}$$
(S3)

Take derivative of U_{ij} w.r.t. coordinate α_i . Note that q_i , q_j and dq_j do not depend on α_i . We obtain the expression of force on atom i

$$F_{i,\alpha}(CF) = F_{i,\alpha} + F'_{i,\alpha} \tag{S4}$$

The first term $F_{i,\alpha}$ is the regular electrostatic and polarization forces calculated in the AMOEBA+ framework with charge-flux-updated charges. The second term $F'_{i,\alpha}$ is the chain rule term due to the explicit dependence of charge flux on geometry. Although in the above we only deal with charge-charge interaction, *Equation S4 is valid in permanent multipole-multipole and induced-dipole polarization interaction as in the AMOEBA+ force field*. For more detailed derivation, please read our previous publications. ¹⁻³ In the current implementation, we loop over each bond (two atoms are involved) and angle (three atoms are involved) in the system to derive the second term (Equation S4) in the following. Finally, a term related to the Ewald self-energy is also derived.

A. Force expression of two atoms in a bond

As has been described in the main text, charge flux on atom a and b due to bond stretching is expressed as

$$dq_a = -dq_b = j_b(r_{ab} - r_{ab}^0)$$
 (S5)

After adding the charge flux on each atom, we want to know the force on atom a due to interaction between atom a and j (and the force on atom a due to interaction between atom a and a a

$$U'_{aj} = \frac{q'_a q'_j}{r_{aj}} = \frac{(q_a + dq_a)(q_j + dq_j)}{r_{aj}}$$
(S6.1)

$$U'_{bj} = \frac{q'_b q'_j}{r_{bj}} = \frac{(q_b + dq_b)(q_j + dq_j)}{r_{bj}}$$
(S6.2)

Take derivative w.r.t. coordinate α_a (Equation S6.1) and α_b (Equation S6.2). Keep in mind that small change of coordinate on atom a affects both dq_a and dq_b (same on atom b). We obtain:

$$F'_{a,\alpha} = -(V_a - V_b)\nabla q_a \tag{S7.1}$$

$$F'_{b,\alpha} = -(V_a - V_b)\nabla q_b = -F'_{a,\alpha}$$
 (S7.2)

where the ∇q terms are the derivatives of dq w.r.t. coordinate as follows

$$\nabla q_a = \frac{\partial dq_a}{\partial \alpha_a} = j_b \left(\frac{\alpha_a - \alpha_b}{r_{ab}} \right) \tag{S8.1}$$

$$\nabla q_b = \frac{\partial dq_b}{\partial \alpha_b} = -j_b \left(\frac{\alpha_a - \alpha_b}{r_{ab}} \right) = -\nabla q_a$$
 (S8.2)

In Equation S7.1 and S7.2, the V_a and V_b are potential due to the multipoles, *including permanent monopole, dipole and quadrupole as well as induced dipole* on atom j. In practice, it is convenient to first accumulate the potential on each atom due to other interacting atoms. Then perform the force computation using these expressions.

B. Force expressions of three atoms in an angle

As also has been described in the main text, charge flux on atom a, b and c due to angle bending $(\angle abc)$ and asymmetrical bond stretching is expressed as dq_a , dq_b and dq_c

$$dq_a = j_{\theta 1}(\theta - \theta_0) + j'_{h1}(r_{hc} - r_{hc}^0)$$
 (S9.1)

$$dq_c = j_{\theta 2}(\theta - \theta_0) + j'_{b2}(r_{ab} - r^0_{ab})$$
 (S9.2)

$$dq_h = -(dq_a + dq_c) (S9.3)$$

It is straightforward to write down the expressions for the atom a, b and c for the asymmetrical bond stretching term by referring to Equation S7.1 and S7.2 as

$$F'_{a,\alpha} = -(V_b - V_c)\nabla q_a \tag{S10.1}$$

$$F_{c,a}' = -(V_b - V_a)\nabla q_c \tag{S10.2}$$

$$F'_{b,\alpha} = -(F'_{a,\alpha} + F'_{c,\alpha}) \tag{S10.3}$$

Again, V_a , V_b and V_c are the electrostatic potentials on atom a, b and c due to atom j and ∇q_a , ∇q_b and ∇q_c are expressed as follows

$$\nabla q_a = j'_{b2} \left(\frac{\alpha_a - \alpha_b}{r_{ab}} \right) \tag{S11.1}$$

$$\nabla q_c = j'_{b1} \left(\frac{\alpha_c - \alpha_b}{r_{bc}} \right) \tag{S11.2}$$

$$\nabla q_b = -(\nabla q_a + \nabla q_c) \tag{S11.3}$$

For the angle term in Equation S9.1-9.3, let's assume that three atoms have the following coordinates: $a(x_a, y_a, z_a)$, $b(x_b, y_b, z_b)$ and $c(x_c, y_c, z_c)$. We write some intermediates for convenience: vector $\overrightarrow{ba} = a - b$, vector $\overrightarrow{bc} = c - b$, $\alpha_{ba} = \alpha_a - \alpha_b$, $\alpha_{bc} = \alpha_c - \alpha_b$ (where $\alpha = x, y, z$). So the angle θ can be expressed using arccosine function as

$$\theta = \arccos\left(\frac{\overrightarrow{ba} \cdot \overrightarrow{bc}}{|ba||bc|}\right) = \arccos\left(\frac{(x_{ba}x_{bc} + y_{ba}y_{bc} + z_{ba}z_{bc})}{\sqrt{\left((x_{ba}^2 + y_{ba}^2 + z_{ba}^2)\right)\sqrt{\left((x_{bc}^2 + y_{bc}^2 + z_{bc}^2)\right)}}}\right)$$
(S12)

Then the derivative of dq w.r.t. coordinate α is expressed as

$$\nabla q_{a} = j_{\theta 1} \left(-\frac{r_{ba} r_{bc}}{\sqrt{r_{ba}^{2} r_{bc}^{2} - (\overrightarrow{ba} \cdot \overrightarrow{bc})^{2}}} \right) \left(\frac{\alpha_{bc}}{r_{ba} r_{bc}} - \frac{\alpha_{ba} \overrightarrow{ba} \cdot \overrightarrow{bc}}{r_{ba}^{3} r_{bc}} \right)$$
(S13.1)

$$\nabla q_c = j_{\theta 2} \left(-\frac{r_{ba} r_{bc}}{\sqrt{r_{ba}^2 r_{bc}^2 - \left(\overrightarrow{ba} \cdot \overrightarrow{bc} \right)^2}} \right) \left(\frac{\alpha_{ba}}{r_{ba} r_{bc}} - \frac{\alpha_{bc} \overrightarrow{ba} \cdot \overrightarrow{bc}}{r_{ba} r_{bc}^3} \right)$$
(S13.2)

$$\nabla q_b = -(\nabla q_a + \nabla q_c) \tag{S13.3}$$

So the chain rule terms due to angle bending for atom a, b and c are

$$F'_{a,\alpha} = -(V_a + V_b - V_c)\nabla q_a \tag{S14.1}$$

$$F'_{c,\alpha} = -(V_a + V_b - V_c)\nabla q_c \tag{S14.2}$$

$$F'_{b,\alpha} = -(V_a + V_b - V_c)\nabla q_b \tag{S14.3}$$

Combining Equation S14 with Equation S10, we obtain the final additional force expressions due to angle bending and asymmetrical bond stretching for atom a, b and c

$$F'_{a,\alpha} = -(V_a + V_b - V_c)\nabla q_a^{bnd} - (V_b - V_c)\nabla q_a^{str}$$
 (S15.1)

$$F'_{c,\alpha} = -(V_a + V_b - V_c)\nabla q_c^{bnd} - (V_b - V_a)\nabla q_c^{str}$$
(S15.2)

$$F'_{b,\alpha} = -(F'_{a,\alpha} + F'_{c,\alpha})$$
 (S15.3)

Note in the above equations, we distinguish the charge flux derivative w.r.t. coordinate with bending and stretching superscripts.

C. Ewald self-energy force

As now charges explicitly depend on the atom coordinate, an extra force term for Ewald self-energy (due to charge only) is needed. Self-energy of atom i is expressed as

$$U_i^{self} = f_{const}(q_i^0 + dq_i)^2$$
 (S16)

where the f_{const} is a coefficient applied to the Ewald self-energy. It is convenient if we define a "self-potential" on atom i due to i as

$$V_i^{self} = 2f_{const}(q_i^0 + dq_i) = 2f_{const}q_i'$$
(S17)

By referring to Equation S7.1-7.2, we obtain the chain rule term for when we loop over each bond

$$F'_{a,\alpha} = -(V_a^{self} - V_b^{self}) \nabla q_a$$
 (S18.1)

$$F'_{b,\alpha} = -F'_{a,\alpha} \tag{S18.2}$$

By referring to Equation S15, we obtain the chain rule term when we loop over each angle

$$F'_{a,\alpha} = -\left(V_a^{self} + V_b^{self} - V_c^{self}\right) \nabla q_a^{bnd} - \left(V_b^{self} - V_c^{self}\right) \nabla q_a^{str} \tag{S19.1}$$

$$F'_{c,\alpha} = -\left(V_a^{self} + V_b^{self} - V_c^{self}\right) \nabla q_c^{bnd} - \left(V_b^{self} - V_a^{self}\right) \nabla q_c^{str}$$
(S19.2)

$$F'_{b,\alpha} = -(F'_{a,\alpha} + F'_{c,\alpha})$$
 (S19.3)

As can be seen from Equation S7, S15 and S19, the chain rule terms are very compact in form. In the code implementation, the subroutines looping over each bond and angle can be reused by both the electrostatics and the polarization, in both real and reciprocal space. This makes it easy to implement modular and clean computer code in Tinker,⁴ Tinker-OpenMM ⁵ and Tinker-HP. ⁶ We have examined the agreement of *numerical and analytical* gradients (negative force) due to electrostatics and polarization energy to ensure the correctness of our implementation.

II. Computational details

A. Liquid simulation in ForceBalance parametrization

ForceBalance automatic parametrization was performed targeted on both the gas phase and liquid phase properties. ForceBalance uses the statistical formula to express the average values of thermodynamic properties and their analytical derivatives. FB has been used in various force field re-parametrization, including our previous AMOEBA+ water potential. ⁷ Much more details about FB can be found in the previous publications. ⁸⁻¹¹ Briefly, in FB optimization, analyze executable was used to compute the energy of gas-phase water clusters and liquid trajectory MD simulations. In the calculation of static dielectric constant, net dipole moments were also computed using analyze program by an additional "M" (for multipole) option. Liquid simulations in NPT ensemble were performed in the CUDA platform using dynamic_omm program. As a compromise of efficiency and accuracy, the box size was chosen to be ~26×26×26 ų containing 590 water molecules. This allows us to use a vdW cutoff of 10 Å, with a long-range correction. Long-range electrostatic interaction was treated using particle mesh Ewald (PME) with 7 Å real space cutoff, which was also used as the cutoff for calculating charge penetration correction. RESPA integrator, ¹²⁻¹³ BUSSI thermostat, ¹⁴ Monte Carlo barostat and 1 fs integrating time step were used

in the NPT simulations. In each FB iteration, 500 ps of equilibration NPT simulation was first performed to equilibrate the water box. Then 5 ns of the production run was performed to calculate the physical properties and gradients *w.r.t.* the parameters.

B. Self-diffusion constant simulation

The self-diffusion constant of water could be underestimated in a limited size of water box in simulations. As in our previous publication, we used five cubic box sizes, 18, 26, 40, 60 and 90 Å, where N_{water} is 216, 590, 2210, 7500 and 25150, respectively, to run NPT simulations using DYNAMIC_OMM.X program. The time length of the simulations is 6 ns, 6ns, 5 ns, 4 ns and 3 ns, respectively. The size-independent self-diffusion constant was obtained by a linear fit to $D \sim \frac{1}{L}$ and extrapolating to $\frac{1}{L} = 0$. Simulation settings are the same as the above (A: Liquid simulation in ForceBalance parametrization). Exceptions are the vdW cutoff used for different sizes of boxes: 7, 10, 12, 12 and 12 Å for five box sizes 18, 26, 40, 60 and 90 Å, respectively.

C. Infrared spectra liquid simulation

The 18 Å water box containing 216 water molecules was used in the IR spectra simulations for AMOEBA03, AMOEBA14, AMOEBA+ and AMOEBA+(CF) water models. A tight convergence criterion for the induced dipole was used (*polar-eps 10*⁻⁷). An integrating time step of 0.5 fs was used and the trajectory was saved every 2 steps (1 fs). The infrared spectra were calculated from the Fourier transforms of the time correlation function of net dipole moments. Three quantum correction approaches suggested by previous work were tested to obtain the final IR intensity. A python-script by Braun was used in IR calculations. ¹⁵ Consistent with the previous work, we found that the $\frac{\beta\hbar\omega}{1-\exp(-\beta\hbar\omega)}$ formula works the best on water. ¹⁶ Thus the corrected intensity by using this approach was compared with experiment through the whole studies.

D. Ice simulation

Ice Ih, Ic and II crystal structures were taken from Tinker "example" directory. Prior to the NPT simulation, the structures were optimized to a convergence of 0.01 kcal/mol/Å using either AMOEBA+(CF) or AMOEBA+ water model. NPT simulations were performed at different temperatures (see **Table S11**) and under 1 atm pressure to make the same comparison with other

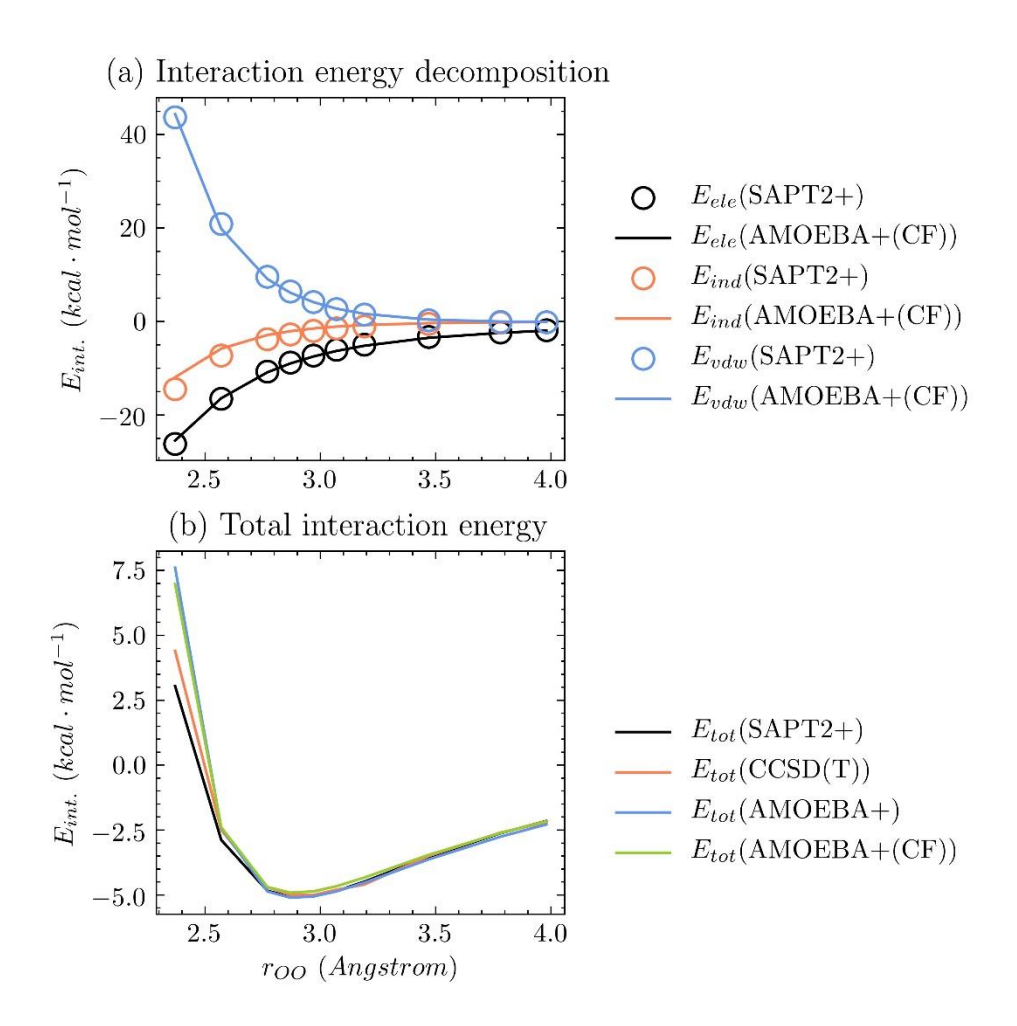
models and experiment. All simulations were performed in the CUDA platform using dynamic_omm program. A cutoff of 9.0 Å for the Ewald real space interactions was used in simulations. Other conditions were kept the same as those in liquid *NPT* simulations. In total 5 ns of trajectory were collected and the final 4 ns was used for analysis.

E. Liquid NVE simulation

Simulation details were kept the same as those in ForceBalance liquid simulations (see above), except that: (1) Prior to NVE simulation, 10-ps of NVT simulation was performed in order to have the initial kinetic energy at 298 K; (2) A cutoff of 9.0 Å was used for the Ewald real space interactions; (3) Both the "OPT4" polarization extrapolation scheme and the SCF iteration scheme were used in the simulations. (4) GPU simulations were performed with Berendsen themostat in an NVT ensemble at 298 K without temperature scaling. This is equivalent to an NVE ensemble.

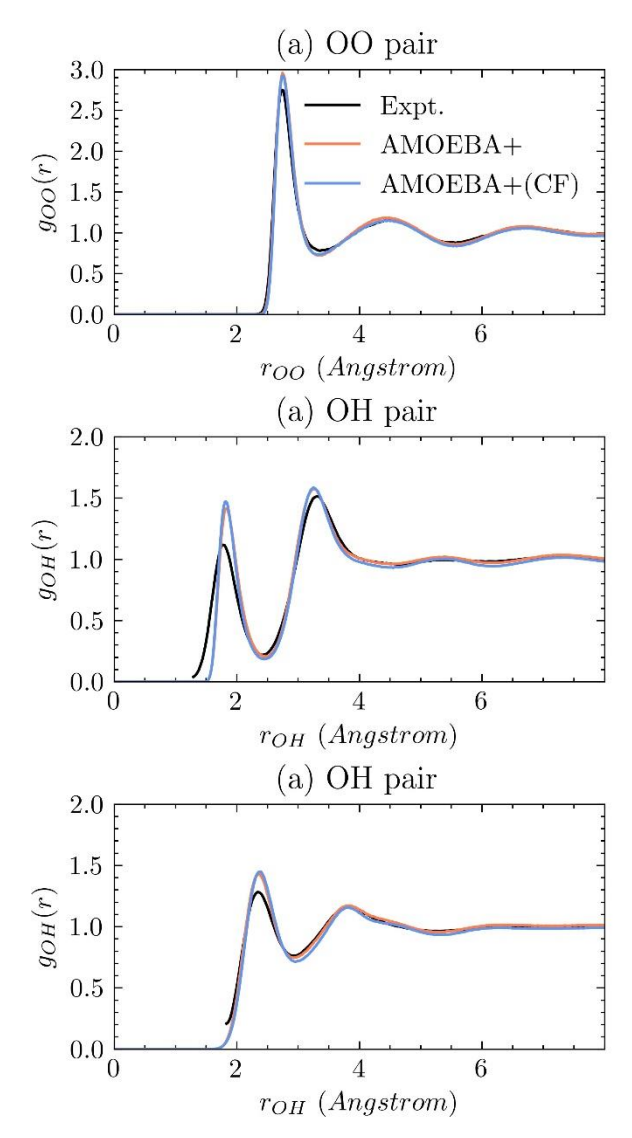
III. Supplementary Figures

Figure S1. The intermolecular interaction energy of hydrogen-bonding dimer.



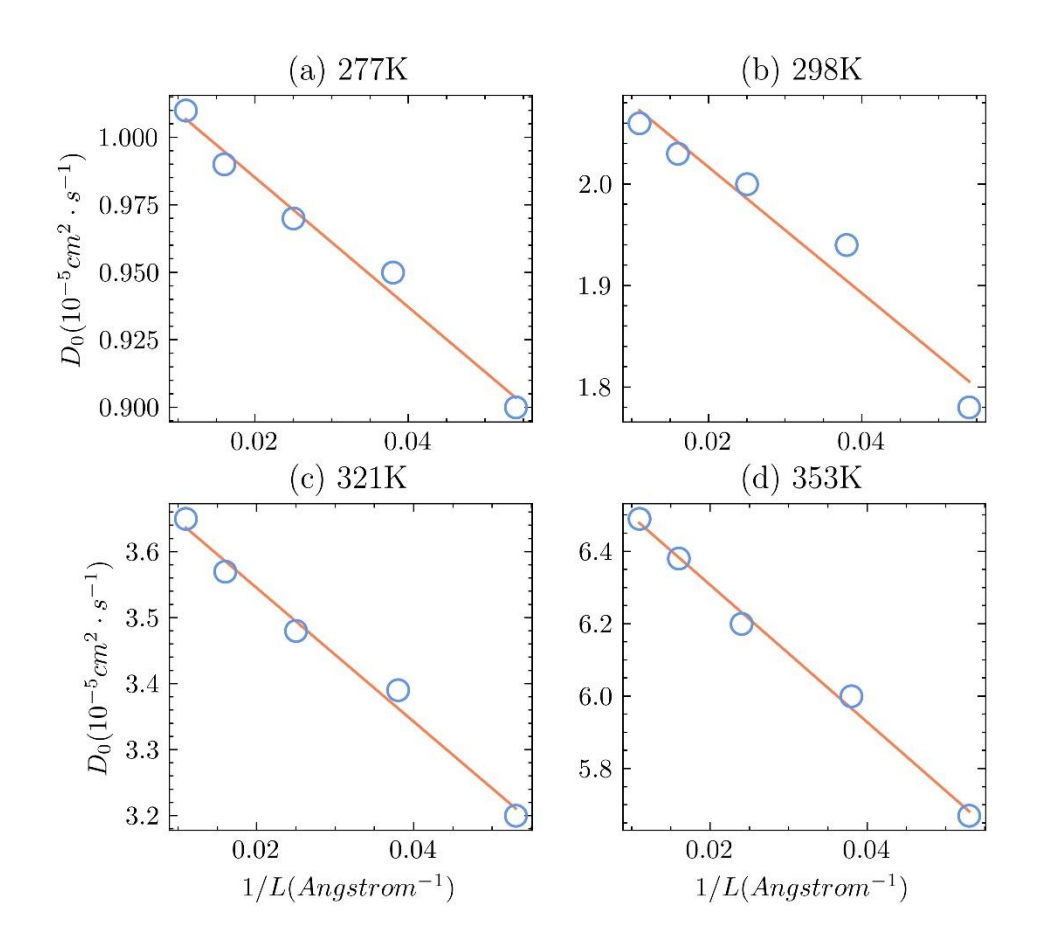
Note: (a) $E_{int.}$ components from SAPT2+ and AMOEBA+(CF) model. (b) Total $E_{int.}$ calculated by two QM methods compared to AMOEBA+ and AMOEBA+(CF) water models.

Figure S2. Radial distribution functions at ambient conditions.



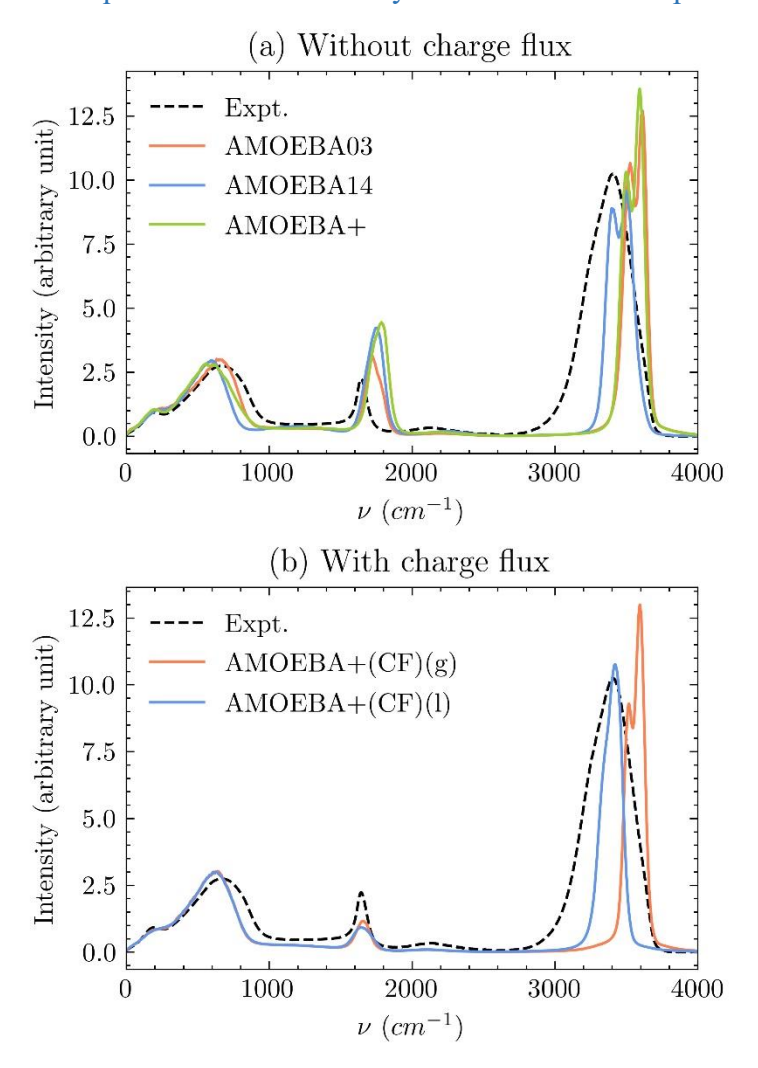
Note: RDFs between intramolecular pairs were not calculated and the experimental data below 1.65 Å (b) and 1.80 Å (c) are not shown on the plot. Experimental data were taken from reference. ¹⁷

Figure S3. The self-diffusion constant of different temperatures and box sizes.



Note: Blue circle: values averaged from different windows of a certain box size. Orange solid line: linear fit of $D_0\sim 1/L$. Final size-corrected D_0 are 1.03, 2.14, 3.75, 6.69 (unit: 10^{-5} cm²·s⁻¹) for 277, 298, 321 and 353 K respectively.

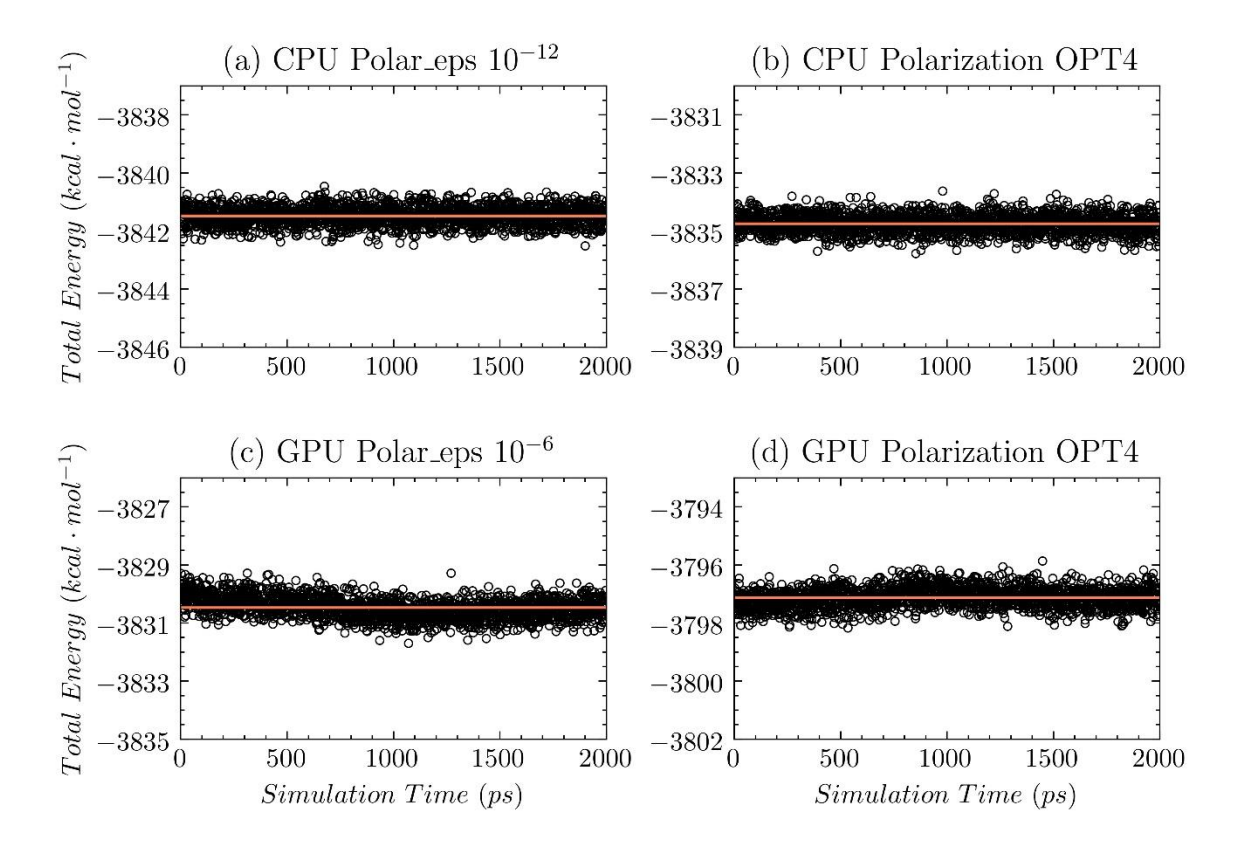
Figure S4. IR spectra of liquid water calculated by various models compared to experiment.



Note: (a) Models without charge flux (b) models with charge flux, where AMOEBA+(CF)(g) uses the force constant using gas-phase optimized OH stretching frequency and AMOEBA+(CF)(l) uses the liquid adjusted frequency. Results from AMOEBA+(CF)(l) is reported in the main text (**Figure 4**).

Figure S5. Energy-time plot of NVE simulations to demonstrate the energy conservation.

(a) and (c): The iterative SCF method was used to solve the *mutual* induction equation with different convergence criteria for induced dipole. (b) and (d): The "OPT4" extrapolation approach was used to solve the *mutual* induction equation. (a) and (b) were calculated on Tinker GPU and (c) and (d) were calculated on Tinker-OpenMM (GPU). The straight line shows the average energy during simulations.



Note: The total energy drifts during simulations were evaluated using a linear fit to the energy-time curves. The drift in total energy is: (a) -0.01 kcal/mol/ns, (b) -0.03 kcal/mol/ns, (c) -0.2 kcal/mol/ns and (d) +0.1 kcal/mol/ns.

IV. Supplementary Tables

Table S1. Optimal parameters of AMOEBA+ and AMOEBA+(CF) water models.

Term	Parameter	Unit	AMOEBA+ a	AMOEBA+(CF)
Multipole	O monopole	e	-0.558246	-0.504458
_	O dipole Z	e·bohr	-0.144923	0.209422
	O quadrupole XX	e·bohr²	0.451599	0.111520
	O quadrupole YY	e·bohr²	-0.280108	-0.316006
	O quadrupole ZZ	e·bohr²	-0.171491	0.204486
	H monopole	e	0.279123	0.252229
	H dipole X	e·bohr	0.000000	-0.149358
	H dipole Z	e·bohr	-0.230060	-0.173051
	H quadrupole XX	e·bohr²	0.215207	0.085256
	H quadrupole YY	e·bohr²	-0.029761	-0.040495
	H quadrupole ZZ	e·bohr²	0.185446	-0.044761
	H quadrupole XZ	e·bohr²	0.191100	-0.073786
CP	O damping factor	none	4.0483	4.0047
	H damping factor	none	3.2748	3.2541
CT	O parameter a_{CT}	10 ³ kcal·mol ⁻¹	3.2003	3.1506
	O parameter b_{CT}	Å-1	3.7188	3.8982
	H parameter a_{CT}	10 ³ kcal·mol ⁻¹	2.9436	2.9229
	H parameter b_{CT}	Å-1	4.7135	4.6867
Polarization	O polarizability	Å	0.948	0.976
	H polarizability	Å	0.416	0.428
	direct damping factor	none	0.70	0.70
	mutual damping factor	none	0.39	0.39
vdW	O vdW diameter	Å	3.808992	3.811532
	O vdW epsilon	kcal·mol-1	0.061361	0.082864
	H vdW diameter	Å	3.340781	3.327841
	H vdW epsilon	kcal·mol-1	0.004571	0.002684
	H vdW reduction	none	0.983604	0.986304
Bonded	O-H bond length	Å	0.94	0.95
	Bond force constant	kcal·mol ⁻¹ ·Å ⁻²	556.85	558.64
	H-O-H angle	degree	108.81	104.54
	Angle force constant	kcal·mol ⁻¹ ·rad ⁻²	48.70	50.11
	U-B H-H length	Å	-7.60	-12.44
	U-B force constant	kcal·mol ⁻¹ ·Å ⁻²	1.53	1.50
Charge flux	bond length, b_0 , b'_0	Å		0.9572
<u> </u>	CF constant, j_b	e∙Å ⁻¹	None	-0.0303
	angle, θ_0	degree (°)	INOHE	104.5
	CF constant, j_{θ}	e·degree ⁻¹		0.0020
	CF constant, j_h'	e·Å-1		-0.0453

a. AMOEBA+ parameters are taken from our previous work. 7

Table S2. The binding energy of water trimer to 17-mers.

These data were used to plot Figure 2a-c. All energies are in kcal·mol⁻¹.

Cluster	Index ^a	QM ^b	AMOEBA+ a	MB-UCB ^c	AMOEBA+(CF) a
Trimer	1	-15.74	-16.08	-16.07	-15.97
Tetramer	2	-27.40	-27.70	-27.88	-27.91
Pentamer	3	-35.93	-35.87	-37.23	-36.18
Prism	1	-45.92	-45.69	-43.11	-46.60
Cage	2	-45.67	-45.92	-44.07	-46.64
Bag	3	-44.30	-44.72	-44.06	-45.10
Cyclic Chair	4	-44.12	-44.00	-46.43	-44.02
Book1	5	-45.20	-45.43	-45.09	-45.80
Book2	6	-44.90	-45.74	-44.49	-45.80
Cyclic Boat1	7	-43.13	-43.19	-45.01	-43.43
Cyclic Boat2	8	-43.07	-42.81	-44.83	-43.35
N16_4444A	1	-164.12	-161.12	-166.63	-163.99
N16_4444B	2	-163.76	-160.57	-165.49	-163.43
N16_BOAT_A	3	-163.71	-161.43	-167.92	-162.97
N16_BOAT_B	4	-163.65	-161.16	-166.45	-162.80
N16_ANTIBOAT	5	-163.44	-160.85	-166.45	-162.60
N17_SPHERE	6	-174.44	-171.35	-180.68	-173.85
N17_5525	7	-174.12	-170.11	-181.16	-172.72
RMSE		0.00	1.89	2.95	0.67

a. Binding energy is calculated in Tinker software by using force field optimized geometry for clusters and monomer. In the end, the optimized monomer has a total potential energy of *zero*. So the binding energy is the "*Total Potential Energy*" of the output of the Tinker *analyze* program.

b. All QM data are CCSD(D)/CBS and taken from references: see AMOEBA+ paper for the cluster from trimer to hexamers and 16 to 17-mers from a separated reference. ¹⁸

c. MB-UCB data are taken from reference. 19

Table S3. The interaction energy of water tetramer, pentamer and hexamer conformers.

These data are used to plot Figure 2d-f. All energies are in kcal·mol⁻¹.

Clusters	Cluster Index ^a	CCSD(T)/CBS a	AMOEBA+ b	AMOEBA+(CF) b	MB-pol ^a
Tetramer	1	-28.81	-30.40	-29.07	-28.55
	2	-27.94	-28.83	-28.37	-27.76
-	3	-24.88	-25.78	-24.65	-24.78
Pentamer	1	-37.93	-39.57	-38.07	-37.42
-	2	-36.64	-38.61	-36.98	-36.40
-	3	-36.48	-38.11	-36.62	-36.34
-	4	-36.17	-37.76	-36.19	-36.07
-	5	-35.47	-37.81	-35.95	-35.31
-	6	-34.79	-37.19	-35.39	-34.65
-	7	-34.10	-36.23	-34.70	-34.02
Hexamer	1	-48.24	-50.51	-48.50	-48.17
-	2	-47.95	-49.63	-48.42	-47.85
-	3	-47.52	-49.35	-47.83	-47.00
-	4	-47.26	-48.78	-47.79	-46.81
-	5	-46.80	-48.50	-47.02	-46.30
	6	-46.47	-48.27	-46.02	-45.63
-	7	-45.44	-46.70	-45.29	-44.76
	8	-45.36	-46.68	-45.21	-44.76
1	RMSE	1	1.74	0.36	0.39

a. These indices and energies are taken from the MB-pol paper. ²⁰

b. The interaction energy of AMOEBA+ and AMOEBA+(CF) are directly obtained from *analyze* program of Tinker software as indicated by "*Intermolecular Energy*" in the output.

Table S4. Size-corrected self-diffusion constant D_0 at four temperatures and 1 atm.

All D_0 values are in $\times 10^5$ cm²·s⁻¹.

Temperature (K)	Expt.	AMOEBA+	AMOEBA+(CF)
277.15	1.28	1.13	1.03
298.15	2.30	2.23	2.14
321.15	3.82	3.85	3.75
353.15	6.57	6.74	6.70

Note: see AMOEBA+ paper for the experimental origin and methodologies to calculate the self-diffusion constant.⁷

Table S5. Liquid density at a broad range of temperatures from 265 to 369 K and 1 atm.

All density values are in kg·m³.

Temperature (K)	Expt.	AMOEBA+	AMOEBA+(CF)
265.15	998.6	996.5	995.9
273.15	999.8	999.3	999.2
277.15	1000.0	1000.0	1000.1
281.15	999.8	1000.4	1000.4
289.15	998.9	1000.3	1000.1
298.15	997.0	998.3	998.4
309.15	993.7	994.7	994.6
321.15	988.9	989.1	988.8
333.15	983.2	982.4	981.6
345.15	976.6	974.2	973.4
353.15	971.8	968.4	967.3
369.15	961.2	955.4	954.1

Table S6. Enthalpy of vaporization at temperatures from 265 to 369 K and 1 atm.

All enthalpy of vaporization is in kcal·mol⁻¹.

Temperature (K)	Expt.	AMOEBA+	AMOEBA+(CF)
265.15	10.8	11.1	11.1
273.15	10.8	11.0	11.0
277.15	10.7	10.9	11.0
281.15	10.7	10.9	10.9
289.15	10.6	10.7	10.8
298.15	10.5	10.6	10.6
309.15	10.4	10.5	10.5
321.15	10.3	10.3	10.3
333.15	10.2	10.2	10.2
345.15	10.0	10.0	10.0
353.15	9.9	10.0	9.9
369.15	9.8	9.7	9.7

Note: see AMOEBA+ paper for the experimental origin and methodologies to calculate the enthalpy of vaporization.⁷

Table S7. Thermal expansion coefficient at temperatures from 265 to 369 K and 1 atm.

All thermal expansion coefficient values are in 10^{-4} K⁻¹.

Temperature (K)	Expt.	AMOEBA+	AMOEBA+(CF)
265.15	-2.4	-5.0	-5.7
273.15	-0.7	-2.2	-2.8
277.15	0.0	-1.5	-1.4
281.15	0.6	-0.6	-0.3
289.15	1.6	1.3	1.2
298.15	2.6	2.7	2.5
309.15	3.5	4.2	4.4
321.15	4.4	5.0	5.4
333.15	5.2	6.7	6.4
345.15	6.0	7.1	7.9
353.15	6.4	8.0	8.0
369.15	7.3	9.3	9.1

Note: see AMOEBA+ paper for the experimental origin and methodologies to calculate the thermal expansion coefficient.⁷

Table S8. Isothermal compressibility at temperatures from 265 to 369 K and 1 atm.

All isothermal compressibility values are in 10⁻⁶ bar⁻¹.

Temperature (K)	Expt.	AMOEBA+	AMOEBA+(CF)
265.15	55.9	60.1	61.1
273.15	52.2	55.9	56.1
277.15	50.7	53.9	54.4
281.15	49.3	52.3	53.0
289.15	46.9	51.6	50.8
298.15	45.2	49.0	51.0
309.15	44.4	49.5	50.2
321.15	44.2	49.2	51.0
333.15	44.5	49.6	51.5
345.15	45.3	51.3	53.9
353.15	46.1	54.3	54.9
369.15	48.3	58.1	59.2

Note: see AMOEBA+ paper for the experimental origin and methodologies to calculate isothermal compressibility.⁷

Table S9. Isobaric heat capacity at temperatures from 265 to 369 K and 1 atm.

All isobaric heat capacity values are in cal·mol⁻¹·K⁻¹.

Temperature (K)	Expt.	AMOEBA+	AMOEBA+(CF)	Quantum Corr.
269.15	18.3	20.6	22.6	-2.5
275.15	18.2	20.6	22.1	-2.4
279.15	18.1	20.1	21.5	-2.4
285.15	18.1	19.8	21.5	-2.3
293.65	18.0	19.6	20.6	-2.2
303.65	18.0	19.5	20.9	-2.1
315.15	18.0	19.2	20.3	-2.0
327.15	18.0	19.2	20.3	-1.9
339.15	18.0	19.6	20.0	-1.8
349.15	18.0	19.3	20.4	-1.7
361.15	18.1	20.0	20.2	-1.6

Note: see AMOEBA+ paper for the experimental origin and methodologies to calculate isobaric heat capacity as well as the quantum corrections.⁷ The calculated data are obtained with the liquid enthalpy of vaporization data using numerical differentiation approach.

Table S10. Static dielectric constant at temperatures from 265 to 369 K and 1 atm.

Temperature (K)	Expt.	AMOEBA+	AMOEBA+(CF)
265.15	91.2	102.3	91.3
273.15	87.9	93.4	90.5
277.15	86.3	89.8	87.2
281.15	84.7	87.2	85.5
289.15	81.7	86.4	83.1
298.15	78.4	79.4	78.8
309.15	74.6	73.2	73.4
321.15	70.6	67.8	70.1
333.15	66.8	64.5	66.0
345.15	63.2	58.8	60.8
353.15	60.9	55.9	58.2
369.15	56.6	52.9	53.9

Note: see AMOEBA+ paper for the experimental origin and methodologies to calculate static dielectric constant.⁷

Table S11. Density of three forms of ice under 1 *atm* pressure and indicated temperatures.

Density of experiment and other models were taken from reference.²¹

Ice	T(K)	TIP5P	SPC/E	TIP4P	TIP4P/Ew	TIP4P/Ice	AMOEBA+	AMOEBA+	Expt.
								(CF)	
Ih	250	0.976	0.944	0.937	0.935	0.909	0.937	0.940	0.920
Ic	78	1.026	0.971	0.964	0.960	0.929	0.968	0.966	0.931
II	123	1.284	1.245	1.220	1.219	1.183	1.260	1.236	1.170

Table S12. Simulated geometrical and energetic properties for ice Ih at 269 K and 1 atm.

Properties	T (K)	TTM2-F ^a	TTM4-F ^a	AMOEBA+	AMOEBA+	Expt.
					(CF)	
θ _{HOH} (°)	269	107.6	109.6	106.0±4.4	106.3±4.4	109.5, ^b 107.0 ^c
r ₀₀ (Å)	269			2.73	2.73	2.75 ^b
$r_{\mathit{OH}}(ext{Å})$	269	0.97	0.98	0.95 ± 0.02	0.97 ± 0.02	0.98 °
ΔH _{sub} (kcal/mol)	269	-13.39	-14.40	-11.99	-12.13	-12.20 °

- a. Taken from reference.²²
- b. Taken from reference.²³
- c. Taken from reference. ²⁴
- d. Taken from reference.²⁵
- e. Taken from reference. ²⁶

References

- 1. Ren, P. Y.; Ponder, J. W., Polarizable atomic multipole water model for molecular mechanics simulation. *J. Phys. Chem. B* **2003**, *107* (24), 5933.
- 2. Rackers, J. A.; Wang, Q.; Liu, C.; Piquemal, J.-P.; Ren, P.; Ponder, J. W., An optimized charge penetration model for use with the AMOEBA force field. *Phys. Chem. Chem. Phys.* **2017**, *19* (1), 276.
- 3. Ren, P.; Wu, C.; Ponder, J. W., Polarizable Atomic Multipole-based Molecular Mechanics for Organic Molecules. *J Chem Theory Comput* **2011**, *7* (10), 3143.
- 4. Rackers, J. A.; Wang, Z.; Lu, C.; Laury, M. L.; Lagardère, L.; Schnieders, M. J.; Piquemal, J. P.; Ren, P.; Ponder, J. W., Tinker 8: Software Tools for Molecular Design. *J Chem Theory Comput* **2018**, *14* (10), 5273.
- 5. Harger, M.; Li, D.; Wang, Z.; Dalby, K.; Lagardere, L.; Piquemal, J. P.; Ponder, J.; Ren, P., Tinker-OpenMM: Absolute and relative alchemical free energies using AMOEBA on GPUs. *J Comput Chem* **2017**, *38* (23), 2047.
- 6. Lagardère, L.; Jolly, L. H.; Lipparini, F.; Aviat, F.; Stamm, B.; Jing, Z. F.; Harger, M.; Torabifard, H.; Cisneros, G. A.; Schnieders, M. J.; Gresh, N.; Maday, Y.; Ren, P. Y.; Ponder, J. W.; Piquemal, J. P., Tinker-HP: a massively parallel molecular dynamics package for multiscale simulations of large complex systems with advanced point dipole polarizable force fields. *Chem Sci* **2018**, *9* (4), 956.
- 7. Liu, C.; Piquemal, J.-P.; Ren, P., AMOEBA+ Classical Potential for Modeling Molecular Interactions. *J. Chem. Theory Comput.* **2019**, *15* (7), 4122.
- 8. Laury, M. L.; Wang, L. P.; Pande, V. S.; Head-Gordon, T.; Ponder, J. W., Revised Parameters for the AMOEBA Polarizable Atomic Multipole Water Model. *J Phys Chem B* **2015**, *119* (29), 9423.
- 9. Qiu, Y.; Nerenberg, P. S.; Head-Gordon, T.; Wang, L.-P., Systematic Optimization of Water Models Using Liquid/Vapor Surface Tension Data. *J. Phys. Chem. B* **2019**, *123* (32), 7061.
- 10. Wang, L. P.; Head-Gordon, T.; Ponder, J. W.; Ren, P.; Chodera, J. D.; Eastman, P. K.; Martinez, T. J.; Pande, V. S., Systematic improvement of a classical molecular model of water. *J Phys Chem B* **2013**, *117* (34), 9956.
- 11. Wang, L. P.; Martinez, T. J.; Pande, V. S., Building Force Fields: An Automatic, Systematic, and Reproducible Approach. *J Phys Chem Lett* **2014**, *5* (11), 1885.
- 12. Humphreys, D. D.; Friesner, R. A.; Berne, B. J., A Multiple-Time-Step Molecular Dynamics Algorithm for Macromolecules. *J Phys Chem* **1994**, *98* (27), 6885.
- 13. Qian, X.; Schlick, T., Efficient multiple-time-step integrators with distance-based force splitting for particle-mesh-Ewald molecular dynamics simulations. *J. Chem. Phys.* **2002**, *116* (14), 5971.
- 14. Bussi, G.; Zykova-Timan, T.; Parrinello, M., Isothermal-isobaric molecular dynamics using stochastic velocity rescaling. *J Chem Phys* **2009**, *130* (7), 074101.
- 15. https://zenodo.org/badge/DOI/10.5281/zenodo.154672.svg
- 16. Gaigeot, M.-P.; Sprik, M., Ab Initio Molecular Dynamics Computation of the Infrared Spectrum of Aqueous Uracil. *J. Phys. Chem. B* **2003**, *107* (38), 10344.
- 17. Soper, A. K., The radial distribution functions of water and ice from 220 to 673 K and at pressures up to 400 MPa. *Chem Phys* **2000**, *258* (2-3), 121.
- 18. Sahu, N.; Singh, G.; Nandi, A.; Gadre, S. R., Toward an Accurate and Inexpensive Estimation of CCSD(T)/CBS Binding Energies of Large Water Clusters. *J Phys Chem A* **2016**, *120* (28), 5706.
- 19. Das, A. K.; Urban, L.; Leven, I.; Loipersberger, M.; Aldossary, A.; Head-Gordon, M.; Head-Gordon, T., Development of an Advanced Force Field for Water Using Variational Energy Decomposition Analysis. *J. Chem. Theory Comput.* **2019**, *15* (9), 5001.
- 20. Reddy, S. K.; Straight, S. C.; Bajaj, P.; Pham, C. H.; Riera, M.; Moberg, D. R.; Morales, M. A.; Knight, C.; Götz, A. W.; Paesani, F., On the accuracy of the MB-pol many-body potential for water: Interaction energies, vibrational frequencies, and classical thermodynamic and dynamical properties from clusters to liquid water and ice. *J. Chem. Phys.* **2016**, *145* (19), 194504.

- 21. Abascal, J. L. F.; Sanz, E.; Fernández, R. G.; Vega, C., A potential model for the study of ices and amorphous water: TIP4P/Ice. *J. Chem. Phys.* **2005**, *122* (23), 234511.
- 22. Burnham, C. J.; Anick, D. J.; Mankoo, P. K.; Reiter, G. F., The vibrational proton potential in bulk liquid water and ice. *J. Chem. Phys.* **2008**, *128* (15), 154519.
- 23. Kuhs, W. F.; Lehmann, M. S., The structure of the ice Ih by neutron diffraction. *J. Phys. Chem.* **1983**, 87 (21), 4312.
- 24. Ichikawa, K.; Kameda, Y.; Yamaguchi, T.; Wakita, H.; Misawa, M., Neutron-diffraction investigation of the intramolecular structure of a water molecule in the liquid phase at high temperatures. *Mol. Phys.* **1991**, *73* (1), 79.
- 25. Whalley, E., Energies of the phases of ice at zero temperature and pressure. *J. Chem. Phys.* **1984**, 81 (9), 4087.
- 26. Feistel, R.; Wagner, W., Sublimation pressure and sublimation enthalpy of H2O ice Ih between 0 and 273.16K. *Geochim. Cosmochim. Acta* **2007**, *71* (1), 36.